ANCHORAGE STRENGTH OF TENSILE STEEL IN REINFORCED CONCRETE BEAMS

by

George Edward Warren

A Dissertation Submitted to the

Graduate Faculty in Partial Fulfillment of

The Requirements for the Degree of

DOCTOR OF PHILOSOPHY

Major Subject: Structural Engineering

Approved:

Signature was redacted for privacy.

In Charge of Major Work

Signature was redacted for privacy.

Head of Major Department

Signature was redacted for privacy.

Dean of Graduate College

Iowa State University
Of Science and Technology
Ames, Iowa

1969

TABLE OF CONTENTS

	Page
INTRODUCTION	1
General Remarks	1
Previous Investigations and the 1963 ACI Building Code	4
Object	5
Scope	6
Notation	8
TEST PROGRAM	12
Description of Bond Specimen	12
Pilot Tests and Design of Specimens	16
Materials	18
Fabrication, Casting, and Curing	19
Test Equipment and Testing Procedure	20
TEST RESULTS	23
Introduction	23
Beam Behavior and Failure Modes	23
Calculation of Stresses	31
Magnitudes of Bond Strength for Top Bars and Effect of Variables	33
Bottom Bars and Modulus of Rupture Tests	37
Effect of Redistribution	38
Anchorage Design Equation Considering Redistribution	41
ANCHORAGE STRENGTH ANALYSIS	50
Introduction	50
Development of an Ultimate Shear Equation for Anchorage Failure	51

	Page
SUMMARY AND CONCLUSIONS	64
ACKNOWLEDGEMENTS	67
LITERATURE CITED	68
APPENDIX A	70
APPENDIX B: PHOTOELASTICITY INVESTIGATION OF RADIAL STRESSES	93
Introduction	93
Models and Loading Arrangement	94
Results	95

INTRODUCTION

General Remarks

All reinforced concrete construction is based on the assumption that the steel and concrete are thoroughly bonded together. Of the three parts of a beam - the web, the compression zone, and the tensile steel - bond action of reinforcement is a major cause of weakness for the tension steel. In extending concrete's application as a structural material, limitation must be placed on its flexural capacity if it cannot develop proper bond strength between concrete and reinforcing steel.

Bond stress is the name assigned to the shear stress along and parallel to the interface between reinforcing steel and concrete. Bond stress is caused by a change in steel stress. The term "flexural bond" identifies the nominal bond stress induced by the transfer between concrete and steel of the change in bar tension and is calculated by $V/\Sigma o j d$. "Anchorage bond" is simply the average bond stress between a point of maximum or peak steel tensile stress to the end of the reinforcing bar where the tensile stress is zero. In some cases these are numerically equal. However, by definition, the tests of this investigation were for determination of anchorage bond.

The problem of bond strength was recognized in the early development of reinforced concrete construction. Since the nineteenth century emphasis has been placed on determining and clarifying variables which affect bond. Thus, bars with lugs were recognized as superior in improving bond over plain bars. Bent and twisted bars were also promoted. Although deformed bars have greatly extended the flexural capacity of reinforced concrete, they have also greatly complicated bond analysis. Lugs of deformed bars add resistance

by wedging and shearing actions to the resistance already available with plain bars: friction and adhesion.

Associated with the shearing stress of bond is a normal radial stress. This latter stress is due to wedging and bearing action of the lugs in their attempt to override the concrete between them. These two types of stresses and their resultant are illustrated in Fig. 1. The normal radial component produces high tangential tensile stresses in the concrete at the interface of the concrete and the steel. This causes splitting in the concrete cover longitudinally along the bar. The shearing bond stress, while holding the bar in equilibrium, tends to produce diagonal cracks at an oblique angle to the longitudinal bars.

Bond failure may occur in the following ways. Due to the expansion in the widths of the longitudinal splitting and diagonal cracking, the bar lugs can override the concrete cast between them. The second type of failure occurs if the cracking is retarded in some manner such as by normal pressure due to reactions or by excess stirrups. Then, the concrete between the lugs is sheared off. In either case the stress transfer capacity at the interface of the concrete and steel is reached and failure of the beam will ensue. With deformed bars the greatest contributing factor to the ultimate bond capacity is the ability of the concrete to resist the lug forces.

Since splitting has long been recognized as an important factor in anchorage failures, information on the influence of bar spacing, beam width, and shear reinforcement is required. Due to the increased use of high strength steel with yield stresses in excess of 75 ksi and lack of knowledge of bond strength with higher steel stresses, further investigation of the influence of embedment length and steel stresses up to 75 ksi on bond is

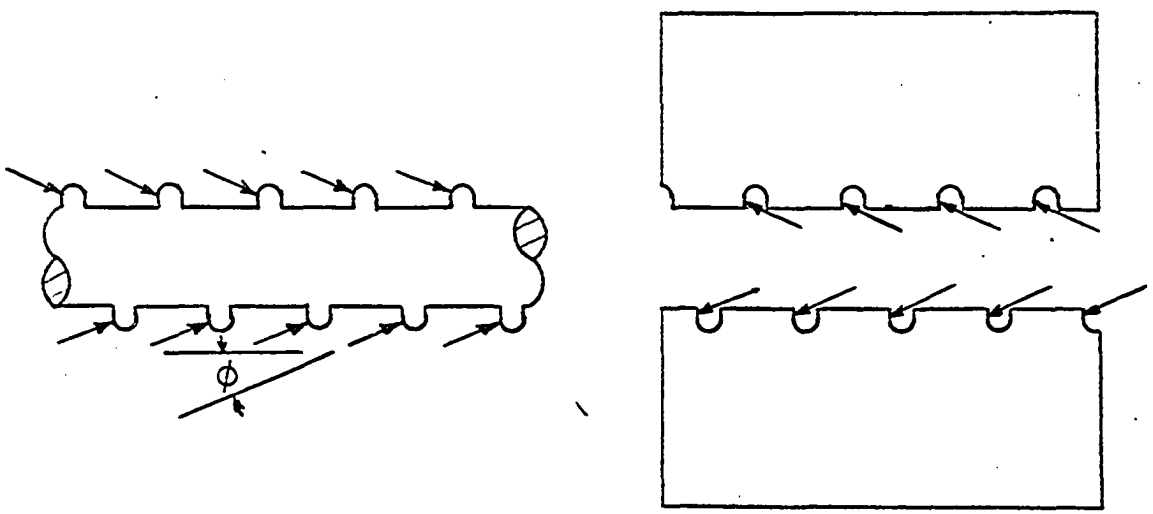

On Bar

On Concrete

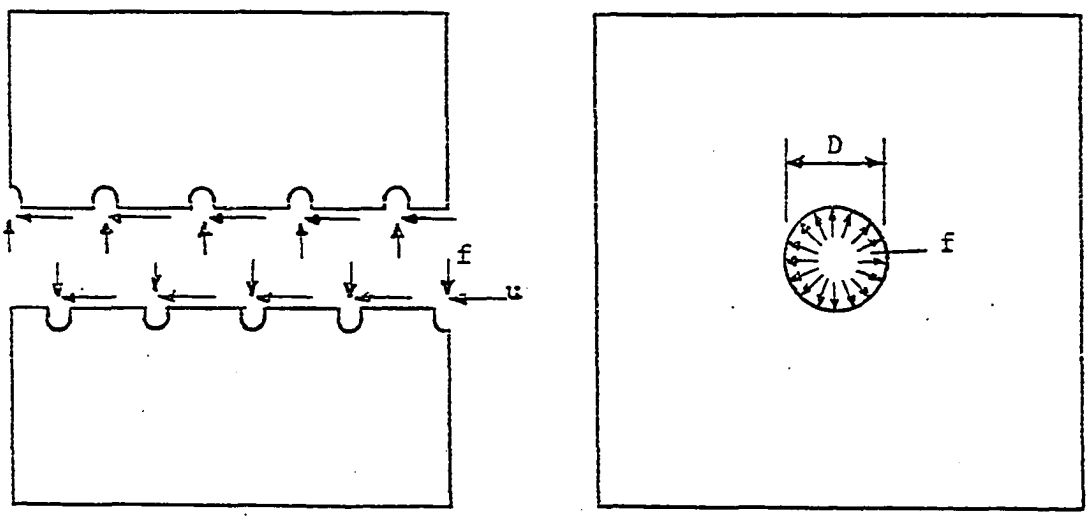

Components

Radial Components

Fig. 1. Bond stress components

needed.

Previous Investigations and the 1963 ACI Building Code

The current ACI Code design allowables (1) are based upon investigations employing specimens which included beams, pull-out, modified pull-out, and half beams that utilized only one or two bars. These tests cannot give adequate information on the influence of such factors as bar spacing and beam width.

Several bond studies have been performed at the University of Texas (4, 7, 8, 9). However, most tests were made with a low steel percentage value. Although the University of Texas tests did not cover all variables that are required, they contributed much to the understanding of bond strength under the influence of low shear stress in the order of $2\sqrt{f'_c}$. Further tests are required in which the shear stress range is from $2\sqrt{f'_c}$ to $10\sqrt{f'_c}$.

Previous research at Iowa State University has shown that normal external pressure, such as that induced by supports, significantly increases the bond strength of deformed bars (10, 11). Such pressure prevents the bar lugs from slipping over the concrete and prevents the concrete from splitting off after cracking. Also transverse reinforcing will affect the bond strength (13, 14). Stirrups serve as crack arresters and as the concrete splits, tensile stresses are transmitted from the concrete to the transverse steel.

One research project at the University of Texas (9) and two at Iowa State University (3, 15), have concluded that close bar spacing is detrimental to bond strength. However, the tests were performed with specimens containing only one or two bars.

Factors such as beam width, bar spacing, arrangement of transverse reinforcement, and embedment length are presently not considered in the bond strength equations given in the ACI Building Code. A limiting bar spacing is given in Sec. 804(a) of the Code (1). It states that the minimum clear spacing between bars shall not be less than the nominal diameter of the bar, 1 1/3 times the maximum size of aggregate, nor 1 inch. This requirement is mainly to insure that concrete is placed securely around each bar.

Object

The object of this investigation was to study the ultimate anchorage capacity of reinforced concrete beams with concentrated loads. In particular, it was desired to study the effect of beam width and bar spacing. The primary supposition to be checked by this thesis was that bond strength would be increased by increased bar spacing. Other variables incorporated were embedment length and stirrup arrangement. The embedment length was varied in order to obtain steel stresses that ranged from 30 to 90 ksi to determine the effect of variation of steel stress on bond strength.

The objectives were to be accomplished by the analysis of results of reinforced concrete beams which were designed to simulate an actual continuous structural member. Further, as part of the analysis, the results of a photoelastic study of the normal radial stresses that are shown in Fig. 1 were to be incorporated.

Scope

Tests were made on 33 concrete beams which consisted of 27 bond specimens and 6 plain concrete beams. Specimen behavior was established by study of crack patterns and mode of failure. Tangential stresses in the concrete adjacent to the reinforcing steel were determined in seven photoelastic models of beam cross sections with various bar arrangements. Using the results of these tests, semi-rational expressions to predict anchorage strength were derived.

Top bars

Most tests of this investigation were concerned with top bars. Top bars are defined as horizontal bars so placed that more than 12 inches of concrete is cast in the member below the bar (1).

Twenty-two specimens were tested. Except for pilot test beams 3B46W and 3B38W, the total depth of the beams were 20 inches and the effective depth, d, equaled 17.3 inches. The width varied from 12 to 24 inches. Total depth, effective depth, and width was 19.5, 16.8 and 16 inches respectively for the pilot specimens. High strength, A431 steel, No. 9 bars were incorporated as test bars in all cases. All beams were reinforced with stirrups. Concentrated loading was applied as shown in Fig. 2.

To determine the effect of beam width and bar spacing, beams with widths of 12, 18, and 24 inches were used with an embedment length of 46 inches including an extension of 17.3 inches beyond the moment inflection point. Number 5 stirrups were used at a spacing of 5 inches on center. The number of longitudinal test bars varied from two to four within the 12 inch

width series, from two to six in the 18 inch series, and from three to seven in the 24 inch series. Clear bar spacing varied from 5.5 to 1.1 inches in the 12 inch wide beams, from 11.5 to 1.4 inches in the 18 inch beams, and from 8.2 to 2.0 inches in the 24 inch beams.

To study the effect of embedment length, beams with 18 inch widths were tested. Using 5 longitudinal bars four tests were made with the embedment length varying from 36 to 76 inches. There were also two tests each of 2 and 3 longitudinal test bars with embedment lengths of 35 and 46 inches.

To determine the effect of stirrup size on ultimate bond strength, shear reinforcement was changed from No. 5 stirrups to No. 4's and No. 6's in two 18 inch width specimens. The spacing of the stirrups remained at 5 inches on center. No attempt was made to evaluate the effect of stirrup spacing on bond.

Bottom bars

Bond strength of bottom bars is higher than that of top bars. To determine the difference between the anchorage strength of top and bottom bars, 5 beams of the top bar tests were repeated using bottom cast bars as the test bars. Four 18 inch width and one 12 inch width beams were tested. The 18 inch width specimens consisted of 2 beams with 5 bars and an embedment length, L", equal to 46 and 62 inches, one beam with 4 bars and an L" of 46 inches, and one beam with 3 bars and L" equal to 35 inches. In the 12 inch wide beam two longitudinal bars with an embedment length of 35 inches were used. Stirrup size and spacing were the same as in the top bar tests.

In addition, six plain concrete beams were cast to determine the difference in rupture strength between top and bottom cast concrete. The

depth, width, and length of these beams was 20 inches, 12 inches, and 6 feet respectively. These beams were simply supported and loaded at 1/3 points. The beams were cast from the same concrete mix in one casting.

Photoelastic investigation

The photoelasticity study was a plane stress investigation of the normal radial stresses acting in the cross sections with various bar arrangements for the 12 and 18 inch width series. Seven models of cross sections were tested. Tangential stress concentration ratios were determined at hole boundaries in the models. The contribution of the tangential stresses was used in the derivation of a semi-rational expression to predict ultimate anchorage strength. The test models, loading arrangement, procedure, and results are presented in Appendix B: Photoelasticity Investigation of Radial Stresses.

Notation

Each specimen referred to in this report is designated by a series of numerals and letters such as 3A46V. The first numeral is the number of longitudinal test bars. The letter following the first numeral represents one of the 4 widths tested: A equals 12 inches, B equals 16 inches, C equals 18 inches, and D equals 24 inches. The numerals following the first letter is embedment length in inches. The last letter signifies the stirrup arrangement: V is No. 5's at 5 inch spacing, W is No 5's at 5 1/2 inches, X is No. 5's at 4 inches, Y is No. 6's at 5 inches, and Z is No. 4's at 5 inches. The majority of tests employed No. 5 stirrups spaced at 5 inches. For bottom bar tests, the specimen number is followed by the symbol *.

In addition, the following notation was used:

A_s = area of longitudinal tension reinforcement.

A_v = area of web reinforcement.

b = width of member.

C = compressive force in the concrete stress block.

D = bar diameter.

d = effective depth, the distance from the topmost compressive fiber to the centroid of the tension reinforcement.

E_s = modulus of elasticity of the reinforcing steel.

E_c = modulus of elasticity of concrete.

F = photoelastic fringe order.

f = normal radial component of bond stress, pressure applied to photoelastic model.

f_c = compressive stress in the concrete.

f'_c = ultimate compressive strength of concrete as determined from standard 6 by 12 inch cylinders.

f_s = stress in tension reinforcement.

f_{sr} = stress in tension reinforcement considering redistribution.

f_v = stress in web steel.

f_y = yield stress of reinforcement.

f_σ = material fringe value.

G = maximum tangential stress concentration ratio in the concrete at the interface of the concrete and steel which is equal to the ratio of tangential stress, σ_1, to the radial stress, f.

h = photoelasticity model thickness.

j = ratio of lever arm of internal resisting moment to effective depth.

$K_1 - K_{10}$ = constants used in deriving equations.

L'' = embedment length.

L' = embedment length minus extension beyond point of countraflexure.

M_{ext} = applied external bending moment.

M_{sup} = bending moment at edge of support.

M_{ult} = bending moment at ultimate load.

N = number of longitudinal test bars.

n = E_s/E_c, ratio of modulus of elasticity of steel to that of concrete.

p = A_s/bd.

P_{ult} = ultimate applied machine load.

q = $\frac{A_s}{bd}\frac{f_s}{f'_c}$.

r = A_v/bs.

S = clear longitudinal bar spacing.

s = stirrup spacing, center to center.

u_{ult} = ultimate bond or anchorage stress.

u_{ur} = bond strength considering redistribution.

V_c = allowable ACI concrete shear capacity.

V_{cap} = shear capacity.

V_{code} = allowable ACI shear capacity.

V_{ult} = ultimate shearing force.

v = shear stress, V/bd.

σ_1, σ_2 = principal stresses.

σ_x = horizontal normal stress.

σ_y = vertical normal stress.

τ_{xy} = shear stress.

ϕ = angle between shear and normal components of bond stress.

Σo = summation of perimeters.

TEST PROGRAM

Description of Bond Specimen

Many types of test specimens have been devised to determine the bond strength between reinforcing steel and concrete. Since design values for bond strength have depended mainly on test results, the test specimen should simulate the stress conditions of the actual structural member as nearly as possible. The quickest and most convenient bond test to determine relative bond values is the standard pullout test, ASTM Designation C232-62. Some of the other tests that have been devised are the modified pullouts such as those used at Iowa State University (15) and University of Texas (9), half beams at Iowa State College (3), Bureau of Standards beam (12), and the University of Texas cantilever beam (4, 7, 8). The choice of a beam test for this study was influenced by the desire for a realistic correlation between the test specimen and an actual structural member.

With modifications, the specimen used in this investigation was the University of Texas cantilever beam as first reported in 1962 (7) (Fig. 2). The beam and load arrangement is statically determinate and consists of a simple span with a cantilever overhang simulating a section of a continuous structure. The test bars are continuous from the point of maximum moment to a point of cut off beyond the point of zero moment; that is, no bars are cut off at intermediate points. When part of the tension steel in a beam is cut off, complications arise due to lowering of shear strength. Also the test region is relatively free and isolated from external confinement and the effects of stress concentration due to a reaction. It was felt that the University of Texas beam test would give the simplest attainable anchor-

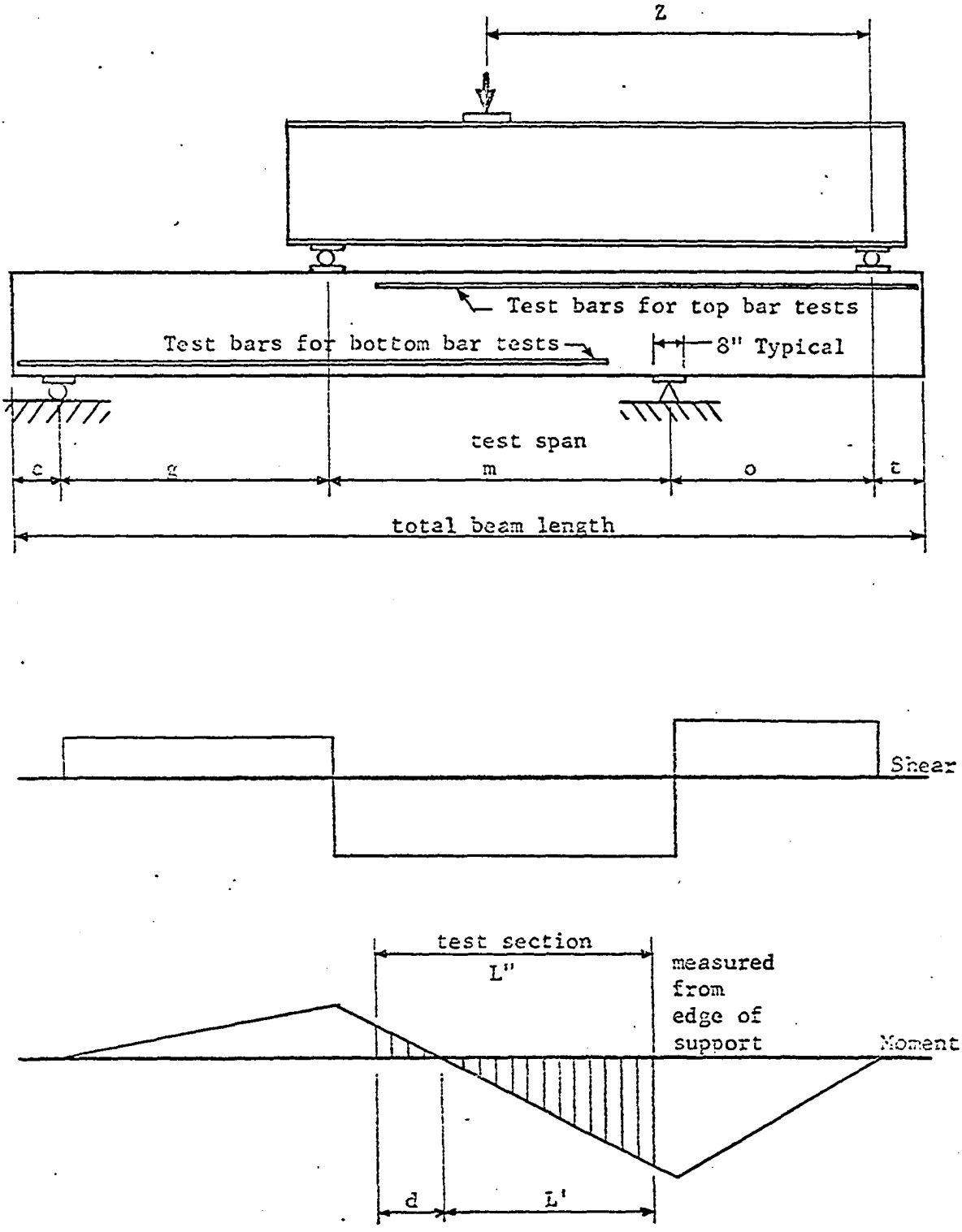

Fig. 2. Load arrangement of test specimen

age conditions along the total development length, L".

The test setup as reported and used by previous investigators (4, 7, 8) had one important weakness which had to be corrected for this study. In previous studies the test bar was cut off at the inflection point for most of the tests. As a result studies were hampered by the detrimental effect of shear and in many cases premature shear failure resulted (7). As a consequence, only specimens utilizing one or two test bars were used. Wide cross sections were used which resulted in many specimens having a low steel ratio, p, that was less than the minimum ACI allowable, $200/f_s$. Cutoffs at points of countraflexure ignore one code requirement (Sec. 918 ACI Code) and, as can be shown, require twice as many stirrups to design for shear.

Assuming diagonal cracking as shown in Fig. 3, the shear equation used now for design of stirrups considers only the summation of the vertical forces.

$$V_{cap} = V_c + \frac{A_v f_v d}{s}$$

where, V_c is the shear carrying capacity of the concrete. Summation of moments about the compressive force yields

$$M_{ext} = f_s A_s jd + \frac{d}{2} \frac{A_v f_v d}{s}$$

In general, the above equation is easily satisfied along a loaded beam; however, at points of cutoff and at points of moment inflection the stirrups can be overstressed, causing a rotational shear failure. In considering the beam specimen of this investigation (Fig. 2), and assuming a diagonal crack passing through the point of countraflexure as shown in Fig. 3,

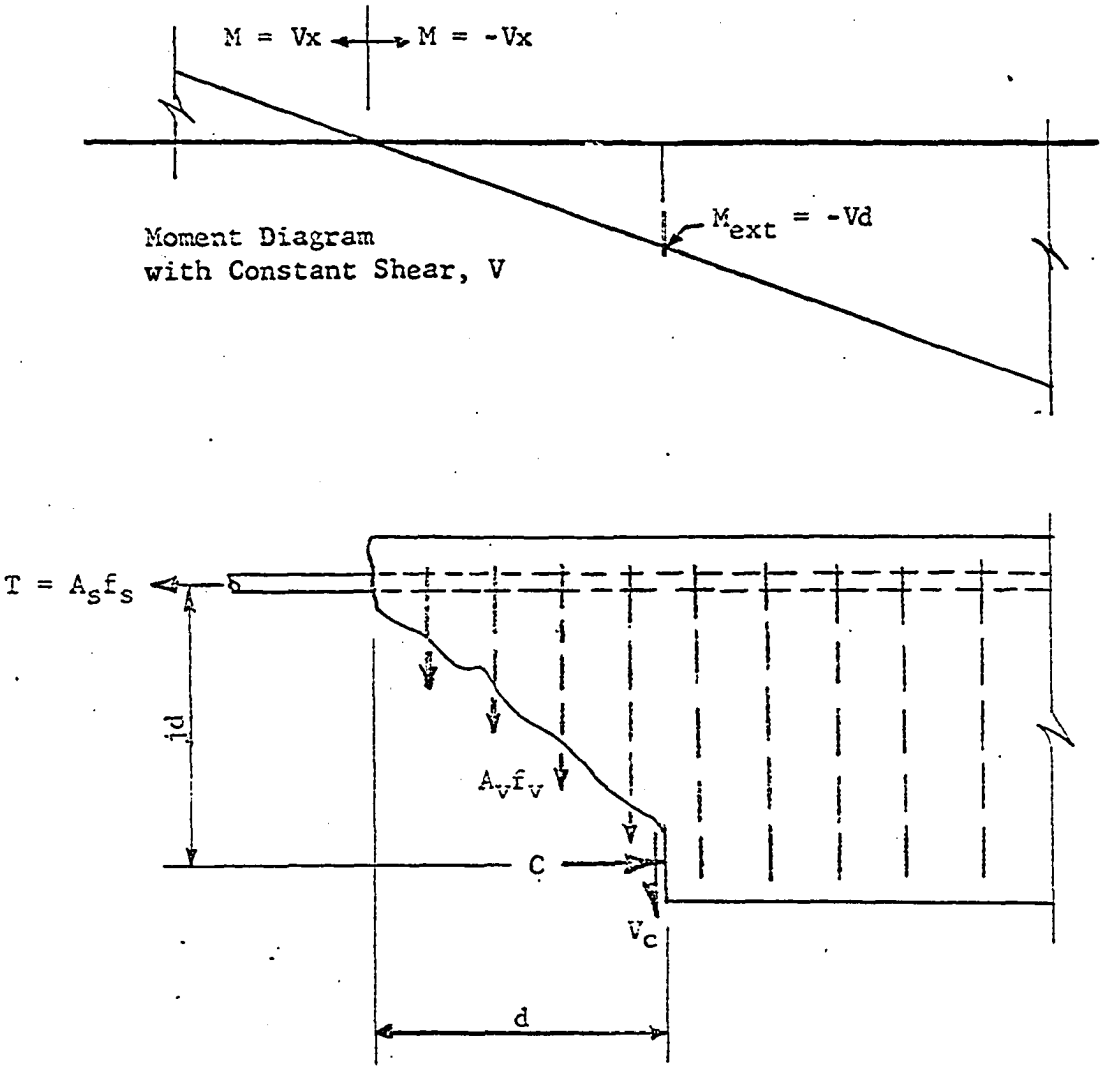

Fig. 3. Internal forces at diagonal crack through point of moment inflection

$$M_{ext} = Vd$$

and

$$V = f_s A_s j + \frac{A_v f_v d}{2s}$$

If there is no extension of longitudinal steel beyond the moment inflection point, then

$$f_s A_s j = 0$$

and

$$V = \frac{A_v f_v d}{2s}$$

Therefore, to develop as much shear as that allowed by the usual design expressions, more than two times as much shear reinforcement is required.

According to Sec. 918 of the ACI Code, there should be an extension of longitudinal tension reinforcement beyond the moment inflection point equal to 12D or d, whichever is greater. The test beams of this investigation satisfied this requirement and the test bars were extended beyond the inflection point by a distance d equal to 17.3 inches.

Pilot Tests and Design of Specimens

Test specimens were designed to fail in anchorage bond with a reasonable margin of safety as far as failure due to shear and flexure. The following ACI Code ultimate strength equations are presently used for design:

Flexure; $M = bd^2 f'_c q(1 - 0.59q)$

where

$$q = \frac{A_s}{bd} \frac{f_s}{f'_c}$$

Shear; $$V_{cap} = v_c bd + \frac{A_v f_v d}{s}$$

where

$$v_c = 1.9\sqrt{f'_c} + \frac{2500pVd}{M}$$

Anchorage Bond;

$$u = 0.8 \frac{6.7\sqrt{f'_c}}{D} \quad \text{Top Bars}$$

$$u = 0.8 \frac{9.5\sqrt{f'_c}}{D} \quad \text{Bottom Bars}$$

See Notation for appropriate symbols.

All the above expressions except those for the allowable anchorage bond strength were used for design of the specimens of this study.

Due to some previous research in which there was no extension beyond the inflection point, some doubt arose as to whether specimens could be designed to fail due to inadequate bond in the laboratory using present code requirements. Therefore, in order to obtain some idea of the order of magnitude of anchorage bond that could be developed, two pilot test specimens were cast, 3B46W and 3B38W. These beams were cast with symetrical positive and negative moment areas in the test span and equal embedment lengths for top and bottom bars. Three longitudinal test bars were utilized in a 16 inch wide and 19 1/2 inch deep cross section. Stirrups within the test span were No. 5's at 5 1/2 inches on center. Other dimensional data are given in Tables 2 and 3 of Appendix A.

Upon successfully attaining an anchorage failure in the top bars with the pilot tests, further beams were designed with the aid of the data obtained. The testing program then proceded on a step by step basis using the information from the beams just tested to plan the next tests. For example, the value of bond, u, used in the design of the second

casting of specimens were approximated from the experimental values of u from the pilot tests. Likewise the u for the third set of beams that were cast was approximated considering the beams of the two previous casting and so forth throughout the program. Knowing u, the corresponding steel stress could be obtained from:

$$f_s = \frac{u \sum oL''}{A_s}$$

Thus, with f_s estimated, the design moment and shear could be determined from the ultimate strength equations.

Materials

The concrete used in this investigation was purchased from a local ready-mix plant. A mix with a 1.0:2.8:3.4 proportion of cement, sand, and aggregate was used with 5 1/2 sacks of cement per yard and 3/4 inch maximum size crushed rock aggregate. Concrete strength varied from 3170 to 4360 psi and slumps ranged from 2 1/2 to 4 1/2 inches. See Table 2 in Appendix A for f'_c, f'_t and slump values for each specimen.

The No. 9 reinforcing bars used as the test bars were purchased from Ceco Corporation and had the same deformation patterns. The test steel conforms to ASTM Designation A431. The stirrups were in conformance to ASTM Designation A15 intermediate grade. All steel was free of oil and grease and had little rust. Typical stress-strain curves for the reinforcing steel are shown in Fig. 26 in Appendix A. Reinforcing steel strengths are tabulated in Table 1 for all specimens.

Fabrication, Casting, and Curing

All specimens were cast in metal forms. Prior to each use the forms were coated with a nonstaining, paraffin form oil to insure easier stripping.

The reinforcing steel was fabricated into a cage with tie wire before placement into the assembled forms. The test bars were positioned such that the longitudinal ribs were oriented in a vertical plane. The stirrups were positioned with the lapped joints of the hoop situated on the side of the beam opposite to the test bars. In this way, the test bars could be tied snugger to the stirrups with the irregularity in the stirrup loop being absorbed in the compression side of the beam.

The cage was placed into the metal forms onto beam bolsters to insure correct uniform concrete cover. Spacers were used to hold the cages in position horizontally. Anchors for lifting the beams were placed outside the test span.

Casting cycle

Prior to casting, a slump test was made and the slump was recorded. The concrete was then placed into the forms and usually half filled before vibrating. The forms were then filled completely and the top half vibrated. Vibration was accomplished with a small laboratory type vibrator with a one inch head which operated at 10,500 vibration per minute.

As the concrete was being placed in the forms, control cylinders were cast in 6 by 12 inch waxed cardboard cylinder molds that were filled with concrete representative of that surrounding the test bars. The control cyl-

inders and specimens were struck off and finished with a trowel.

Curing

After the concrete had set for 5 to 6 hours, the control cylinders and the specimens were covered with wet burlap and sheets of polyethelene. The next day the forms were stripped and the waxed cardboard molds removed from the cylinders. All were given identification marks. The control cylinders were placed near the specimens for similar curing conditions and all were recovered with wet burlap and plastic sheets. The concrete was moist cured until the required strength was reached with the burlap being rewet daily to maintain moisture.

The polyethelene sheets and wet burlap were removed from the concrete after sufficient strength had been developed. Moist curing varied from three days to two weeks. Specimens and control cylinders were allowed to air dry in the laboratory at least one full day prior to the application of strain gages or testing.

Test Equipment and Testing Procedure

A 300,000 pound capacity Southwark Emery hydraulic universal testing machine was used to test concrete control cylinders and representative samples of reinforcing steel. Load to the test beams was applied by a 400,000 pound capacity hydraulic testing machine.

Two SR-4 type A-9-4 strain gages were cemented onto the surface of the concrete cover of the test bars at the calculated point of inflection. These gages were continuously monitored by a Brush amplifier and recorded by an oscillograph throughout loading. From the strain measurements of the gages,

the accuracy of the calculated inflection point was checked and, in addition, the instant in which cracking in the concrete had progressed to the moment inflection point could be determined. This was used as an indication as to when the extension steel began to play a role in resisting an anchorage failure.

Control cylinders

Control cylinders were tested immediately before, during, or just after a specimen test. Compression and splitting tensile tests accompanied all beam specimens.

The compression cylinders were capped with a sulfur-lead compound and tested in accordance with ASTM C39-66 at a rate of 20-50 psi per second. An average of at least three cylinders were used to determine the value of f'_c recorded in Table 2 of Appendix A. Likewise, the splitting tensile tests were made in accordance with ASTM C496-66. An average of three or four tests were used to determine the value of f'_t in Table 2.

Beam tests

The beams were supported on a system of 1/4 inch plywood bearing pads, steel plates, and roller and pin supports. Two point loading was applied through a 24 WF 160 load beam which was positioned over the beam and set on rollers at the points of loading (Fig. 2). The roller and pin supports and the spherical bearing head of the testing machine eliminated any reasonable amount of longitudinal restraint.

With the beam in position, the strain gages were wired to the Brush equipment for continuous recording of strain during loading. After balance

of strain gage bridge, loading was applied.

Loading was applied at the rate of approximately 6000 pounds per minute. The load applied to the beam was marked on the trace of the oscillograph output in increments of 5000 pounds or less or when crack formation occurred. The beams were tested to their ultimate capacity. After testing, the specimens were removed for photographing.

Modulus of rupture beams

The plain concrete beams were set on roller and pin supports (Fig. 27, Appendix A). Concentrated load was applied at 1/3 points through a 10 WF 45 load beam which was supported on rollers. As in the bond specimens, 1/4 inch plywood was used as bearing pads. The beams were loaded to ultimate capacity at a rate of approximately 3000 pounds per minute.

TEST RESULTS

Introduction

In the following sections, the experimental bond strengths, beam behavior, and failure mode will be discussed and described. Test data are presented in the form of tables, curves, and photographs. In general, the following observations were made and recorded for each bond specimen: machine loads for appearance of various crack formations, ultimate machine load, and mode of failure.

A summary of the observed and computed experimental data regarding anchorage strength is presented in Tables 5-7. Rupture beam test data appear in Table 8.

Tables 1 and 2 contain properties of materials used in the specimens. In Table 1, the strengths of reinforcing steel are tabulated, while in Table 2, concrete properties of each beam are listed.

Dimensions of loading arrangements for each beam are recorded in Table 3. Listed in Table 4 are cross sectional properties of the specimens.

Beam Behavior and Failure Modes

Top bars

Similar cracking and behavior developed for most specimens regardless of the variables in consideration. Initial cracking was a moment crack opposite the edge of the support at a section of maximum moment. This crack progressed usually beyond mid-depth of the beam before other cracks would appear. Other flexural cracks developed along the embedment length at reg-

ular spacing as loading continued. A diagonal crack formed next and joined a flexural crack at approximately a distance d from the edge of the support. When the applied load had reached at least half of the ultimate, longitudinal splitting began to develop, progressing down the center of the beam and advancing in front of the transverse flexural cracks that had already formed. After approximately 80 percent of the ultimate load, short diagonal or stitch cracking began to form on the side of the beam adjacent to the main diagonal crack at the level of the longitudinal steel (Fig. 4). As loading continued, the stitch cracks continued to develop along the embedment length. At 90 to 100 percent of the ultimate load, stitch cracking had progressed the full length of the embedment. Also, the longitudinal splitting in the concrete cover had spanned the gaps between flexural cracks. At ultimate load the stitch cracks joined together and the concrete split on a horizontal plane through the reinforcement (Fig. 5). Also, the diagonal stitch cracks had extended across the full width of the beam.

At impending failure, major diagonal crack widths were in the order of 0.05 inches while the widths of the initial moment crack averaged 0.03 inches.

As excessive slip in the longitudinal reinforcement became evident, the initial moment crack would cease to increase in width or in some cases would tend to close after ultimate load had been reached. In contrast, the main diagonal crack became progressively wider as did the small diagonal or stitch cracking near it. This suggests that the ultimate anchorage failure occurred from the main diagonal crack out to the end of the embedment length.

Deviation from the usual behavior occurred in the following manner for 3 of the specimens with low steel percentages (2A46V, 2C46V, and 3C46V). In

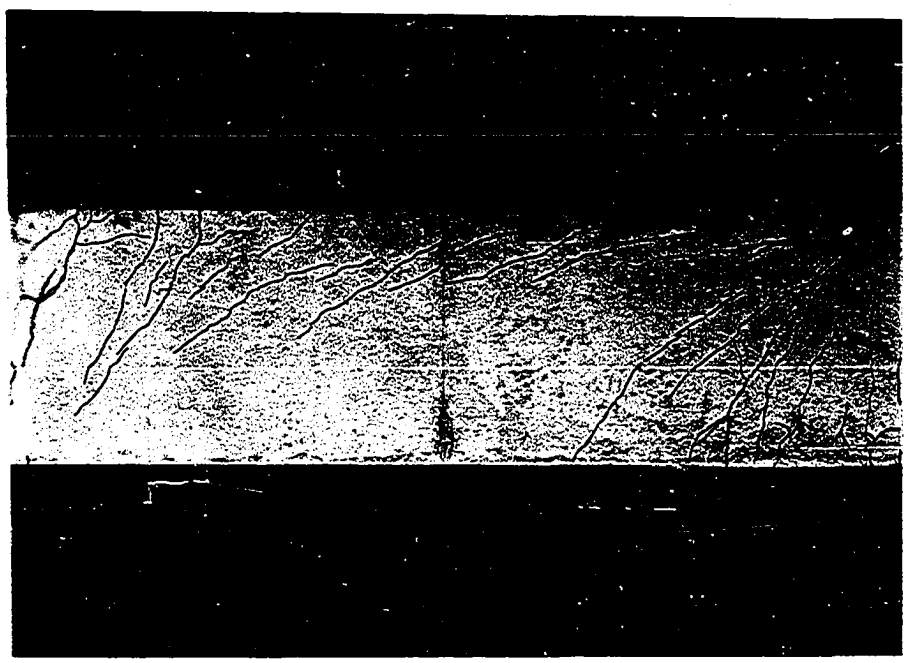

Fig. 4. Short diagonal or stitch cracking (Specimen 2C46V)

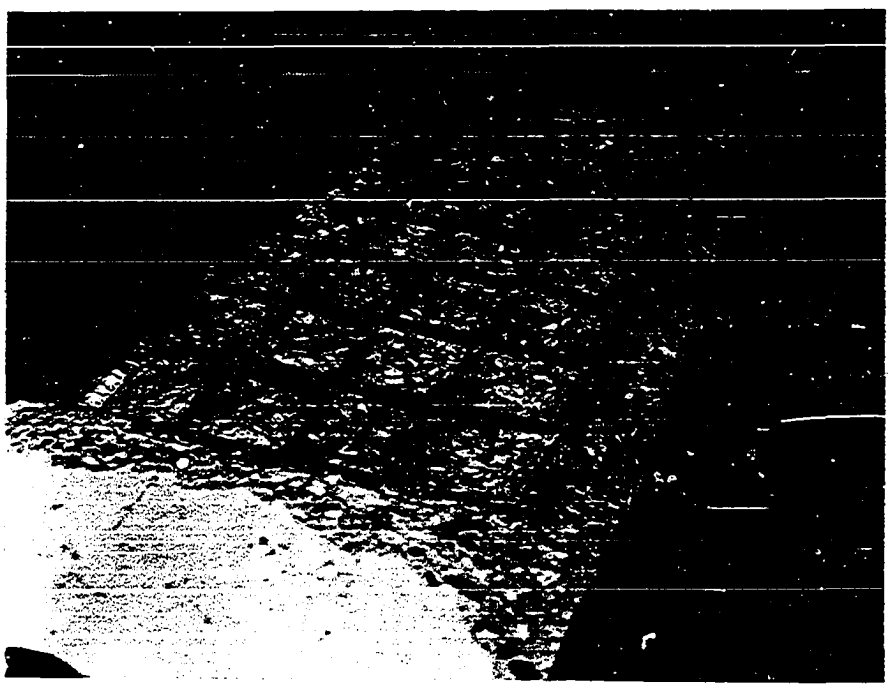

Fig. 5. Final horizontal splitting plane of failure (Specimen 5D46V)

the 2 bar specimens for 12 and 18 inch widths (2A46V and 2C46V, respectively) the major diagonal crack extended enough into the concrete compression zone to cause crushing at the point of maximum moment, at the edge of the support, before anchorage failure occurred. In addition, the yield strength of the longitudinal steel of these two specimens was exceeded before reaching ultimate load. In the 18 inch width specimen with 3 bars (3C46V), the yield strength of the steel was also exceeded before the ultimate anchorage capacity was obtained. However, there was no crushing of the concrete in this specimen. With yielding of the longitudinal steel at maximum moment, the initial moment cracks became excessively wide causing a greater deflection than usual before the ultimate load was reached. The steel stress of all other specimens was below the yield limit of the material at ultimate.

Typical final crack patterns of the anchorage failures obtained in this investigation are shown in photographs in Figs. 6 and 7. Figure 6 indicates the short diagonal or stitch cracking and the main diagonal cracking which had joined flexural cracking at a distance d from the support. Longitudinal splitting and transverse flexural and shear cracking of the concrete cover is shown in Fig. 7. The photograph of Fig. 4 shows the stitch cracks which were typical at 90 to 100 percent of the ultimate load. The difference in the cracking pattern of Fig. 4 and Fig. 6 gives an indication of the relative progress of cracking at the time of failure. The solid horizontal and vertical lines on the beams indicate locations of longitudinal and stirrup reinforcement respectively.

In the beams that had a lower percentage of stirrup steel and wider widths, the progression of cracks along the embedment was more rapid. For the 5 and 6 bar tests of the 24 inch width series (Specimen 5D46V and 6D46V),

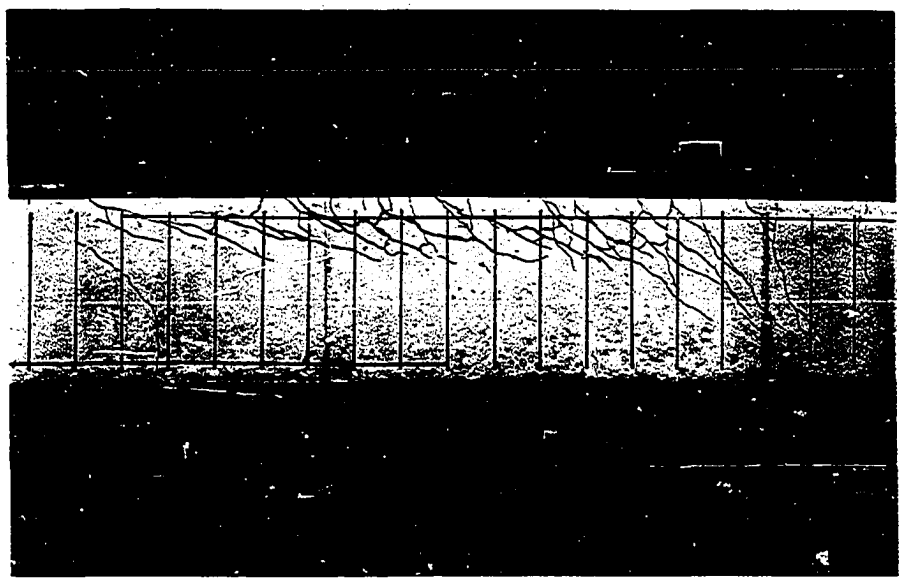

Fig. 6. Diagonal and stitch cracking at failure (Specimen 5C76V)

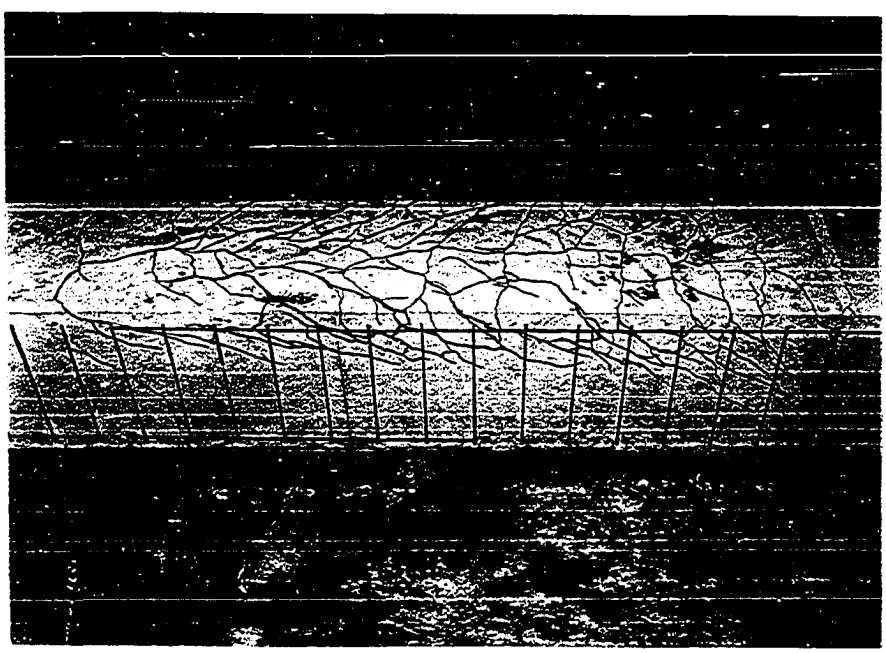

Fig. 7. Transverse cracking and longitudinal splitting at failure (Specimen 5C76V)

there were no stitch cracks before failure. The stitch cracks appeared suddenly and propagated rapidly down the embedment length at ultimate load. After the ultimate load had been attained, the load dropped off rapidly and slippage of steel and crack width became more pronounced.

Although there was a rapid drop in the load carrying capacity after the ultimate load had been reached in Beams 5D46V and 6D46V, none of these beams failed as violently as those with only one test bar and no stirrup reinforcement (15).

Propagation of cracking down the embedment length was slower in the beams containing a higher percentage of shear reinforcement. At ultimate load the splitting and diagonal cracking had already progressed to the end of the embedment. However, after the ultimate load had been attained in these beams, the rate of drop in load carrying capacity was less than that of the specimens with a lower percentage of shear reinforcement. For example, although its tensile steel had not yielded, the 18 inch width specimen with 5 longitudinal bars and No. 6 stirrups (5C46V) sustained an additional deflection of over 2 1/2 inches after attaining ultimate load while still carrying 88 percent of the maximum load. This high deflection was mainly due to slippage of the longitudinal steel. Cracks were as wide as 1/4 inch in the beams having a high percentage of stirrup steel while still carrying at least 80 percent of the ultimate load.

In general, the following observations were made in regard to cracking and the propagation of cracks along the embedment length:

1. The stirrups served as crack arresters and gave the beams more ductility. The higher the percentage of the stirrups; the greater the

ductility of the beam.

2. An increase in the number of bars increased the rate of progression of cracks along the embedment length.
3. An increase in width increased the rate of progression of cracks.
4. A decrease in web steel ratio, r, increased the rate of progression of cracks.

Bottom bars

For the bond tests of bottom bars, stitch cracking progressed along the embedment length of both top and bottom bars. However, the cracks along the top bars progressed ahead of those along the bottom bars. This is because the bond capacity of top bars is less than that for bottom bars. Total anchorage failure of the top bars was prevented by extending them into and beyond the support. Although the top bars did not fail, it cannot be determined as to what effect the excess slipping due to the stitch cracking adjacent to the top bars had on the ultimate anchorage capacity of the bottom bars. The stitch cracks of bottom bars extended further into the beam than those of the top bars (Fig. 8). Also, those stitch cracks which developed adjacent to the main diagonal crack had either joined the major diagonal crack or extended across the web to join the stitch cracks eminating from the top bars. The major diagonal cracks opened wider than those of the top bar tests due to the increased shear. These cracks extended into the compression zone of the concrete.

Due to the main diagonal crack and the stitch cracks along the top bars, notable crushing of the concrete at the support occurred before anchorage failure in the 2 and 3 bar specimens with short embedment (3C35X* and 2A35V*) and the 5 bar specimen with the longer embedment (5C62V*).

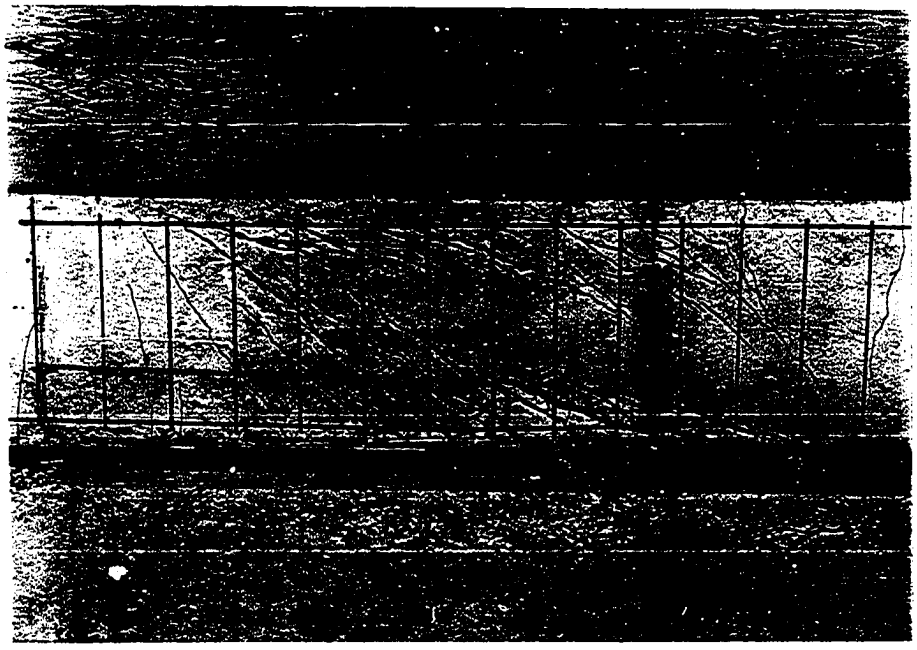

Fig. 8. Bottom bar anchorage failure (Specimen 4C46V*)

Complications due to diagonal cracking and crushing of concrete may have affected the ultimate bond strength of the bottom bar specimens. However, all ultimate failures of the bottom bar specimens involved an anchorage failure of the longitudinal bars. The bond strengths of these tests are at least valid lower bounds.

Calculation of Stresses

The value of ultimate bond strength was computed by

$$u_{ult} = \frac{f_s A_s}{\Sigma o L''} = \frac{f_s D}{4L''}$$

where L'' is the total embedment length and f_s is the steel stress at the edge of the support at ultimate load.

Several researchers in the past have computed the value of f_s from

$$f_s = \frac{M}{A_s jd}$$

with j equal to 7/8 (4, 7, 8, 13). This assumes the internal moment arm to be equal to a constant times the effective depth, d. However, increasing width, b, increases the internal moment arm. Since several different widths were incorporated in this investigation, it was felt necessary to use either ultimate strength or straight line theory in calculating f_s in order to account for the variation of jd.

At low concrete stress, sufficient accuracy can be attained in determining jd by assuming the concrete behaves elastically. Therefore, at low failure loads, f_s was obtained by straight line theory. At higher stresses, near that in which the concrete will crush, a more realistic method of analysis based on the inelastic behavior of concrete must be used. Therefore,

at higher failure loads, f_s was determined from ultimate strength theory. Actually, in all specimens except three beams of the 24 inch wide series with 5, 6, and 7 bars (5D46V, 6D46V, and 7D46V), the f_s values were determined on the basis of ultimate strength theory. In these three cases, the value of the maximum compressive stress in the concrete, f_c, computed by straight line theory was less than $0.8f'_c$. The values of the steel stress, f_s, at ultimate load and the ultimate bond stress, u_{ult}, are recorded in Table 5 of Appendix A.

Adjusted stresses

There was no intention of making concrete strength a variable in this investigation. However, due to different rates of curing, the concrete strengths varied from 3170 psi to 4360 psi. In order that comparisons could be made without the involvement of concrete compressive strength as a variable, all ultimate bond values and steel stress values in Tables 5 and 7 were adjusted to those that would be attributed to an equivalent concrete strength of 4000 psi. Previous research has indicated that ultimate bond strength varies approximately as the square root of the compressive concrete strength (4). Therefore, the following adjustment factor was used:

$$\text{Adjustment Factor} = \sqrt{\frac{4000}{f'_c}}$$

This adjustment factor is tabulated in Table 2 of Appendix A. The value of the factor varied from 0.957 to 1.125.

Magnitudes of Bond Strength for Top Bars and Effect of Variables

Present design values for bond are given as functions of the square root of the concrete compressive strength. However, the experimental bond strength of this investigation varied from 176 psi for specimen 6D46V up to 647 psi for specimen 2C46V while for the same two specimens, $\sqrt{f'_c}$ only changed from 58.4 to 59.3 respectively. Although the square root of the concrete compressive strength cannot be considered as a major variable in this study, bond strength varied nearly 360 percent due to other variables that were involved. This would seem to indicate that further variables should be considered in determining the ultimate strength design values. In all comparisons made below, the ultimate bond strength values were adjusted to those that would be attributed to an equivalent concrete strength of 4000 psi.

Bar spacing, beam width, and number of bars

Variations of the magnitudes of the ultimate anchorage strength for the 12, 18 and 24 inch series with an embedment length of 46 inches are listed below.

For the 12 inch widths, the ultimate bond strength varied from 649 psi for the 2 bar specimen with a clear bar spacing, S, of 5.5 inches (2A46V) to 391 psi for the 4 bar specimen with S equal to 1.1 inches (4A46V). For the 18 inch width, bond varied from 691 psi for the 2 bar specimen with S equal to 11.5 inches (2C46V) to 233 psi for the 6 bar specimen with S equal to 1.4 inches (6C46V). For the 24 inch widths, bond varied from 576 psi for the 3 bar specimen with S equal to 8.2 inches (3D46V) to 215 psi for the 7 bar specimen with S equal to 2.0 inches (7D46V). With the number of bars con-

stant, the ultimate bond strength increased slightly with beam width.

A summary of the results of the 46 inch embedment length tests with 12 to 24 inch widths are plotted in Figs. 18 to 20 in Appendix A. Ultimate bond strength and developed steel stress are plotted against clear bar spacing (Fig. 18), number of bars (Fig. 19), and beam width per bar, b/N (Fig. 20).

Although all of the curves indicate good trends, there is a different curve for each beam width, except possibly in the plot of bond and steel stress versus number of bars (Fig. 19). Bond strength and steel stress increased with increasing clear bar spacing and b/N. However, unit bond stress decreased with increasing number of bars. The ACI anchorage bond allowables for top bars are marked on each figure.

Bond strengths obtained from specimens with 5 or more bars were lower than the ACI allowable design values. The most unsafe value of bond strength obtained was 58 percent of the code value (Specimen 6D46V). Bond values obtained from other tests indicate the ACI Code allowables to be conservative. In several cases the allowables were more than 100 percent conservative (Table 6).

Effect of embedment length

Developed steel stress versus embedment length is plotted in Fig. 21 of Appendix A. The experimental values of steel stress for embedment lengths varying from 36 inches to 76 inches and 18 inch width beam utilizing 5 longitudinal bars are shown. Developed steel stress increased almost linearly from 31.4 ksi for an embedment of 36 inches (Specimen 5C36V) to 88.3 ksi for an embedment of 76 inches (Specimen 5C76V). The corresponding unit

bond stress increased from 246 psi for 5C36V to 343 psi for 5C76V. This represents an increase of the unit bond strength of approximately 2 psi per inch of increase of the embedment length beyond 36 inches.

Similar results were obtained for the 3 bar specimens (3C35X and 3C46V) and the 2 bar specimens (2C35V and 2C46V). Unit bond strength increased from 650 psi (L" = 35 inches) to 691 psi (L" = 46 inches) with the 2 bar specimens and from 502 psi (L" = 35 inches) to 539 psi (L" = 46 inches) with the 3 bar specimens.

An increase in unit bond strength with an increase in embedment length is contrary to results obtained in previous studies. The investigators reported a decrease in unit bond strength with increase in embedment length using specimens with one or two test bars (7, 8).

As the test results indicate (Table 5), the ultimate shear decreased as embedment length increased. Since the shear capacity remained the same, there was decrease in the ratio of ultimate shear to the shear capacity, V_{ult}/V_{code}, ranging from 0.85 for the specimen with a 36 inch embedment length (5C36V) to 0.69 for the 76 inch embedment length specimen (5C76V). One explanation for the rise in the anchorage strength could be due to the decrease of this ratio. However, the shear reinforcement made up approximately 60 percent of the total shear capacity and it will be shown in the next section that changing the stirrup size had little effect. Therefore, possibly the decrease in the shear stress caused the bond strength to increase. At any rate the increase in anchorage strength was accompanied by a decrease in shear stress when the embedment length was increased.

Effect of stirrup size

Experimental results were compared to ACI allowables and ratios of the experimental values to the allowables are tabulated in Table 6. The ratio of V_{ult}/V_{code} varied from 0.94 to 0.52.

To determine if a variation of shear capacity would affect the ultimate anchorage strength, the following tests were conducted. For the five bar specimen with V_{ult}/V_{code} equal to 0.85 and an embedment length of 46 inches (5C46V), the shear reinforcement was increased by changing the No. 5 stirrups to No. 6 stirrups (5C46Y). Likewise, for the five bar specimen with V_{ult}/V_{code} equal to 0.69 and L" equal to 76 inches (5C76V), the No. 5 stirrups were changed to No. 4's (5C76Z). The stirrup size was varied but not the stirrup spacing. Number 4 stirrups represented a 35 percent decrease in shear reinforcement over the No. 5 stirrups while No. 6's were a 30 percent increase. As indicated by the tabulated results (Table 5), there was no increase in the ultimate anchorage strength due to increasing the stirrup size and there was only a 9 percent decrease when the stirrup size was decreased. Although the number of tests were limited, stirrup size seemed to have little effect on the ultimate bond strength.

Effect of extension

As was stated in an earlier section, the extension beyond the point of moment inflection was necessary in order to prevent a rotational shear failure. The percent of ultimate load at which the cracking and splitting had propagated to the point of countraflexure is listed in Table 5 of Appendix A. At this load level, the extension came into play. Additional anchor-

age capacity was available due to the extended steel.

The load at which the extension became effective was determined from strain measurement at the inflection point and visual observation of the crack pattern. Until progression of stitch cracking to the inflection point, strain in the concrete was nearly zero at this point, as was to be expected. However, at the percent of ultimate machine load indicated in Table 5, there was a sudden jump in the strain output. Stitch and, or, longitudinal splitting was instantly visible at the inflection point. This would seem to indicate the instant in which the extension became effective in resistance of an anchorage failure.

Usually the cracking at the inflection point did not occur until after 90 percent of the ultimate load had been applied. This would suggest that an extension equal to the effective depth was of minor importance in increasing significantly the anchorage strength.

Bottom Bars and Modulus of Rupture Tests

With exception of one test value, the bottom bar anchorage strengths were higher than the values from the same tests of top bars. In general, bottom bar bond values averaged 1.12 times those values obtained from top bar tests.

Experimental values of ultimate anchorage strength and steel stress for bottom bars are tabulated in Table 5 of Appendix A. In comparison to ACI bottom bar allowables (Table 6), the experimental results indicate that the allowables were from approximately 20 percent insufficient to 50 percent conservative.

Modulus of rupture test results

Since there is a difference in the anchorage strength of top and bottom bars and anchorage failures are essentially tensile failures of the concrete, modulus of rupture beams were tested to determine the difference in the tensile strength of top and bottom cast concrete. The rupture beams were cast with the same depth as the bond specimens.

All rupture beams failed with a vertical flexural crack inside the 1/3 "pure moment" portion of the beams within 6 inches of the centerline. The flexural strength results are tabulated in Table 8 of Appendix A. The concrete compressive and splitting tensile strength were obtained from an average of 5 control cylinder tests each.

The rupture tensile strength of the bottom cast concrete averaged 444 psi while that of the top cast concrete average 384 psi. In other words, the bottom cast concrete was 1.16 times as strong in tension as the top cast concrete. Although the number of tests are limited, it is interesting to note that the difference in the tensile strength between top and bottom cast concrete is in the same order as the difference between the bond strength of top and bottom bars.

Effect of Redistribtuion

Due to the main diagonal cracking (Fig 6 and 8), the longitudinal steel at a distance d from the edge of the support must resist the moment at the face of the support except for the redistribution of stress to the stirrups. That is, when a diagonal crack is formed, propagating toward the edge of the support, then summation of moments about the compressive force at the

face of the support yields (Fig. 9):

$$M_{sup} = f_{sr}A_s jd + \frac{f_v A_v d^2}{2s}$$

where f_{sr} is the stress in the steel at the section in which the diagonal crack crosses. M_{sup} is the bending moment at the face of the support. To have some indication of the effect of the stirrups on redistribution, $A_v f_v$ is determined from summation of forces in the vertical direction.

$$V_{ult} = V_c + \frac{A_v f_v d}{s}$$

$$\frac{A_v f_v d}{s} = V_{ult} - V_c$$

Substituting this expression into the above equation for M_{sup}:

$$M_{sup} = f_{sr}A_s jd + \frac{d}{2}(V_{ult} - V_c)$$

and

$$f_{sr} = \frac{1}{A_s jd}\left[M_{sup} - \frac{d}{2}(V_{ult} - V_c)\right]$$

where V_c is the shear capacity of the concrete and is obtained from the following ACI empirical expression:

$$V_c = bd\left(1.9\sqrt{f'_c} + \frac{2500Vpd}{M}\right)$$

Upon determining f_{sr} at the section in which the diagonal crack crosses the longitudinal steel, u_{ur} can be determined. In calculating the redistributed bond stress, u_{ur}, the length of embedment is shortened from L" to L" minus d.

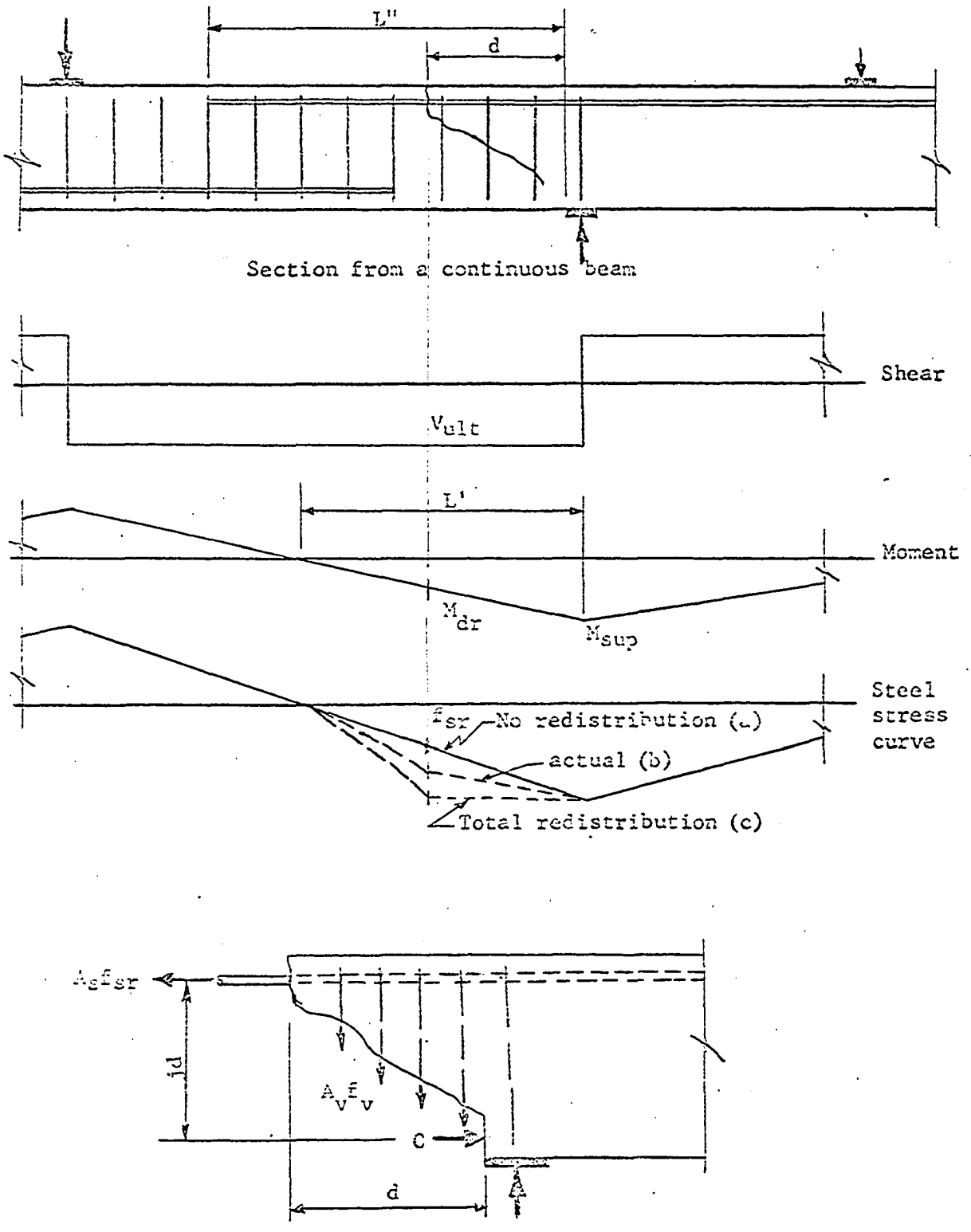

Fig. 9. Redistribution of stress at diagonal cracks

A summary of values for the redistributed steel stresses and anchorage stresses are tabulated in Table 7 and plotted in Figs. 22 - 25 of Appendix A. In the figures, the redistributed bond and steel stress is plotted against clear bar spacing (Fig. 22), number of bars (Fig. 23), and the ratio b/N (Fig. 24). In general, the redistributed anchorage strength increased by approximately 25-30 percent over that obtained using the steel stresses at the edge of the support and the total embedment length. This gives an indication as to the cause of the complete anchorage failure from the diagonal crack to the end of the embedment. Unit anchorage stresses considering redistribution indicate the same trends as to the effect of bar spacing, number of bars, and b/N as for the anchorage stresses computed at the edge of the support (Figs. 18 - 21). However, the effect of the embedment length is less for the redistributed bond values than with the values determined at the edge of the support (Fig. 25) In the specimens with 5 longitudinal bars and 18 inch widths, the redistributed bond strength varied from 340 psi for L" minus d equal to 18.7 inches (5C36V) to 407 psi for L" minus d equal to 58.7 inches (5C76V). This represents an increase in unit bond strength of 1.3 psi per unit length of increase of embedment length above 18.7 inches. Similar results were obtained for the 2 and 3 bar tests.

Anchorage Design Equation Considering Redistribution

Although the maximum steel stress at the section of maximum moment can be evaluated quite simply and safely for any cracked beam, due to inclined cracking, the steel stresses still remain actually quite large at a distance d from maximum moment location (Table 7). For a safe design, the reinforcing must be anchored sufficiently beyond this point to develop the redis-

tributed steel stress.

Shown in Fig. 9 is a typical portion of a continuous beam at an interior support which was simulated in this program with the cantilevered beam. The moment decreases from a maximum at the support to zero at a point of countraflexure. If a diagonal crack joins a flexural crack at a distance from the support and then propagates toward the edge of the support, the following conditions possibly exist:

1. If the shear reinforcement prevents any redistribution of stress caused by diagonal cracking to the longitudinal steel, then for design, f_{sr} can be calculated in the same manner as the steel stress at the cracked section for maximum moment (Fig. 9, steel stress curve a):

$$f_{sr} = \frac{M_{dr}}{A_s jd}$$

where M_{dr} is the moment at a distance d from the edge of the support.

2. If there is no shear reinforcement, there would be a complete redistribution of tensile stresses to the longitudinal steel. Then the steel stress at a distance d from the support would be almost equal to that at the face of the support (Fig. 8, steel stress curve c). However, the embedment length is shortened from L" to L" minus d causing a high concentration of bond stress at the face of the diagonal crack.

3. Nominal stirrup reinforcement to prevent shear failure alone will not prevent all redistribution of stresses due to diagonal cracking. The actual stress at a distance d from the supports is probably somewhere between the two extremes stated above (Fig. 8 steel stress

curve b). To completely retard the redistribution of steel stress, more shear reinforcement than is required to prevent shear failure is needed. Although the stirrups do prevent most of the redistribution, the average anchorage stresses from a distance d out to the end of the embedment is much higher than the average computed from the edge of the support over the full length of L".

Using the results from all the top bar tests, an empirical design equation for steel stress can be derived using the concept of anchorage capacity based on the redistribution of stress at the diagonal crack. The moment at the face of the support can be expressed in terms of the steel stress at a distance d from support plus the contribution of the shear reinforcement.

$$M_{sup} = f_{sr}A_s jd + \frac{A_v f_v d^2}{2s}$$

where

$$f_{sr}A_s = u_{ur}\Sigma o(L'' - d)$$

also

$$\frac{A_v f_v d}{s} = V_{ult} - V_c$$

Therefore, substituting the above expressions into the moment equation yields:

$$M_{sup} = u_{ur}\Sigma o(L'' - d)jd + \frac{d}{2}(V_{ult} - V_c)$$

The moment at the support is usually expressed in terms of the steel stress at the support,

$$M_{sup} = f_s A_s jd$$

or

$$f_s = \frac{M_{sup}}{A_s jd}$$

Therefore,

$$f_s = \frac{u_{ur} \Sigma o}{A_s} (L'' - d) + \frac{V_{ult} - V_c}{2jA_s}$$

A lower bound of f_s can be evaluated by using j equal to 1.00. The value for the anchorage bond, u_{ur}, can be taken from an expression determined from the plot of experimental values shown in Fig. 10:

$$u_{ur} = \frac{2000}{N}$$

If the previous equation is modified to account for bar diameter and f'_c, assuming that bond varies with 1/D and $\sqrt{f'_c}$, then

$$u_{ur} = \frac{35 \sqrt{f'_c}}{ND}$$

and since

$$\Sigma o = N\pi D$$

then

$$f_s = \frac{1}{A_s}\left[110(L'' - d)\sqrt{f'_c} + \frac{1}{2} (V_{ult} - V_c)\right]$$

V_{ult} is the design ultimate shear and V_c is the concrete shear capacity and is assumed to be

$$V_c = bd(1.9 \sqrt{f'_c} + \frac{2500Vpd}{M})$$

A comparison between the steel stress at the support calculated by the above expression and the experimental values can be made with the aid of the

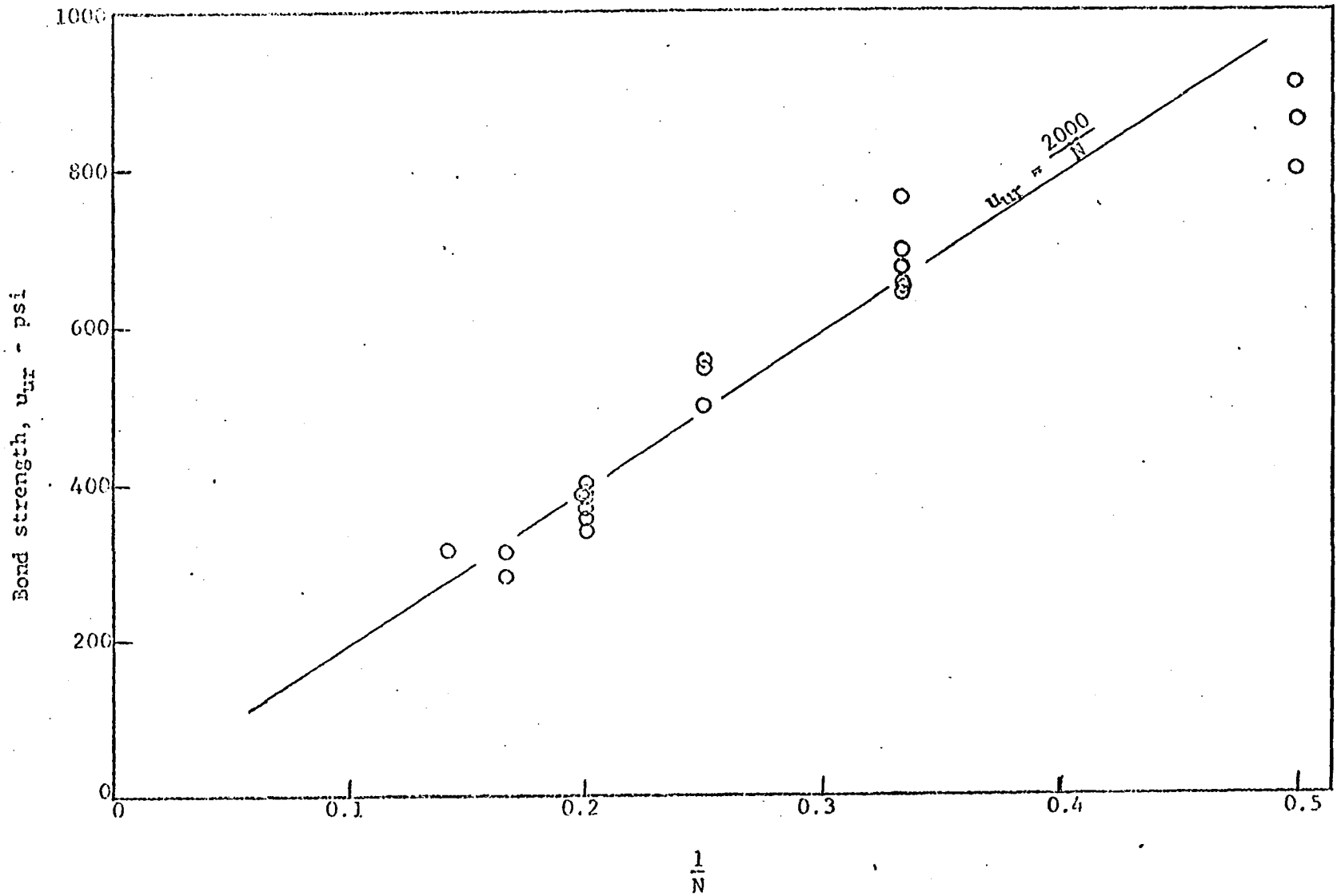

Fig. 10. Redistributed anchorage bond versus the inverse of the number of bars

the plot in Fig. 11.

Bottom bar equation for f_s

Although there may be some difference in beam behavior, such as amount and distribution of slip before and at failure, the ultimate anchorage failures for top and bottom bars of this study were similar in appearance. That is, the ultimate failure was a tensile failure of the concrete surrounding the test bars. Therefore, at least for the type of failure obtained in these studies, it would appear that the difference between the anchorage strength of top and bottom bars would be due mainly to change in concrete tensile strength between top and bottom cast concrete. By using the ratio of the bottom to top cast concrete tensile strength obtained from the rupture tests of this study, the expression for f_s obtained from the top cast bars were altered to consider bottom bars. In the equation, the term which contained the expression for the concrete tensile strength, i.e. $\sqrt{f'_c}$ was multiplied by the value of 1.16.

The expression for developed steel stress utilizing the concept of anchorage failure beginning at a distance d from the maximum moment at the support is altered to the following for bottom bars:

$$f_s = \frac{1}{A_s}\left[128(L'' - d)\sqrt{f'_c} \div \frac{1}{2}(V_{ult} - V_c)\right]$$

In Fig. 12, the experimental values of steel stress at ultimate for the bottom bars is plotted against the above expression for comparison between the two. In general it appears that the above expression is adequate, for the bottom bar tests of this investigation, but there is some scatter which

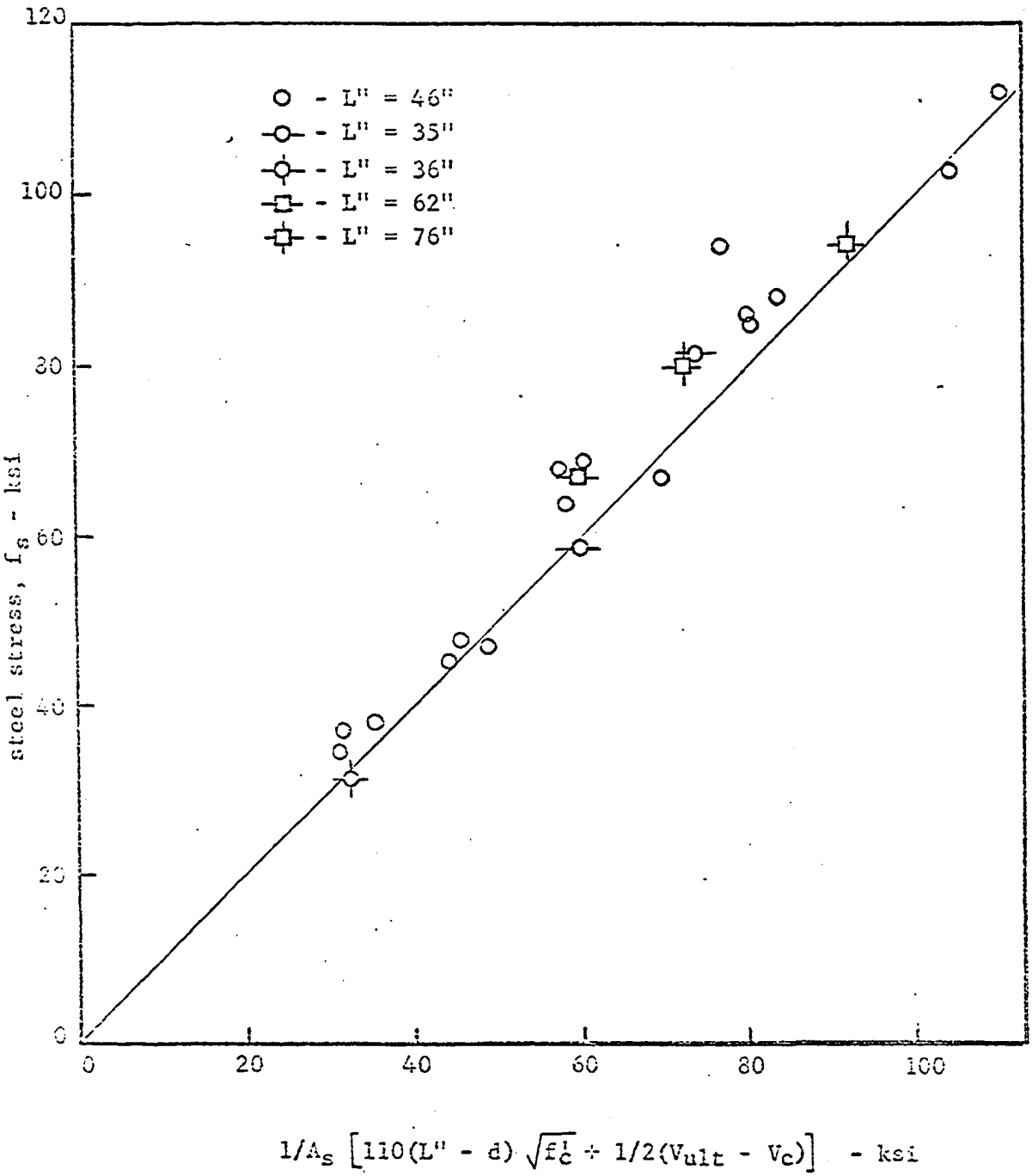

Fig. 11. Experimental versus derived developed steel stress

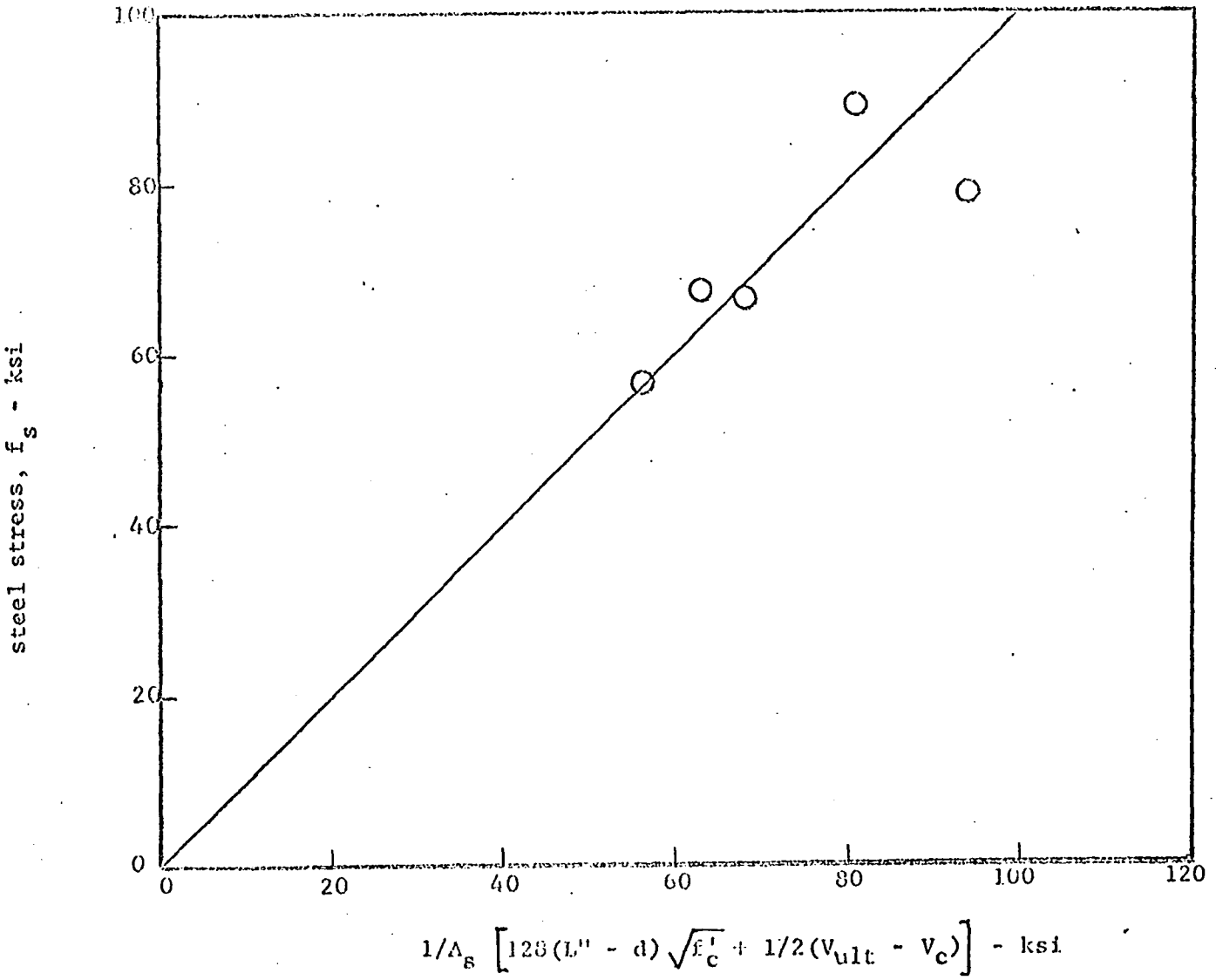

Fig. 12. Experimental steel stress versus derived steel stress - bottom bars

is to be expected with the complications that arose with the failures of the bottom bar specimens.

ANCHORAGE STRENGTH ANALYSIS

Introduction

The object of this portion of the investigation was not to determine an exact theory for failure but to determine the parameters which influence the ultimate anchorage capacity of the longitudinal steel. By semi-rational means, it seemed possible with the aid of the experimental results to obtain parameters and an understanding of the failures on the basis of some theoretical considerations. Any rational analysis of concrete failures is complicated by the nonhomogeniety and nonisotropy of the material. The stress-strain relationship in concrete is influenced by the presence of cracking and steel reinforcement. Failure in reinforced concrete is a progressive one and the distribution of stresses in the concrete is influenced by cracking.

Concepts

Although the ultimate anchorage failure was a horizontal splitting failure on a plane passing through the longitudinal bars, it was always preceded by the formation of short diagonal or stitch cracks in the vicinity of the reinforcing bars (Fig. 4). These cracks formed at later stages of loading. The location and inclination of the cracks indicated that they were caused by excessive principal tensile stresses. The stitch cracks were formed when the concrete tensile strength at the level of the bars was exceeded.

The semi-rational analysis of the anchorage failure was based upon an assumed state of biaxial elastic stress which existed at the time in which the diagonal stitch cracks were formed. The following stresses were assumed

to be acting on an element of concrete adjacent to the reinforcing bar (Fig. 13):

1. flexural concrete stress, σ_{xf}, acting between flexural cracks,
2. shear stress, τ_{xy} ,
3. doweling stress, σ_{yd} , which is caused by the vertical bearing pressure due to the prying action of the reinforcing steel,
4. tangential stress, σ_{yw}, at the interface of the concrete and steel along a horizontal plane passing through the steel; this component of stress was caused by the wedging action of the reinforcing bar lugs.

The distribution of these stresses in the concrete is not known because of the influence of reinforcement and cracking.

Development of an Ultimate Shear Equation for Anchorage Failure

The maximum tensile stress, σ_{max}, is given by the principal stress equation, adjusted to the notation used above:

$$\sigma_{max} = \frac{\sigma_{xf} + (\sigma_{yw} + \sigma_{yd})}{2} + \sqrt{\left[\frac{\sigma_{xf} - (\sigma_{yw} + \sigma_{yd})}{2}\right]^2 + \tau_{xy}^2}$$

The magnitude of the normal bending stress, σ_{xf}, is influenced by the presence of tensile cracks. Hence it cannot be computed on the assumption of an uncracked section. However, neither can it be computed directly from the cracked section theory with any sufficient accuracy. For this analysis, σ_{xf} was assumed proportional to the tensile stress, f_s, computed by the cracked section theory:

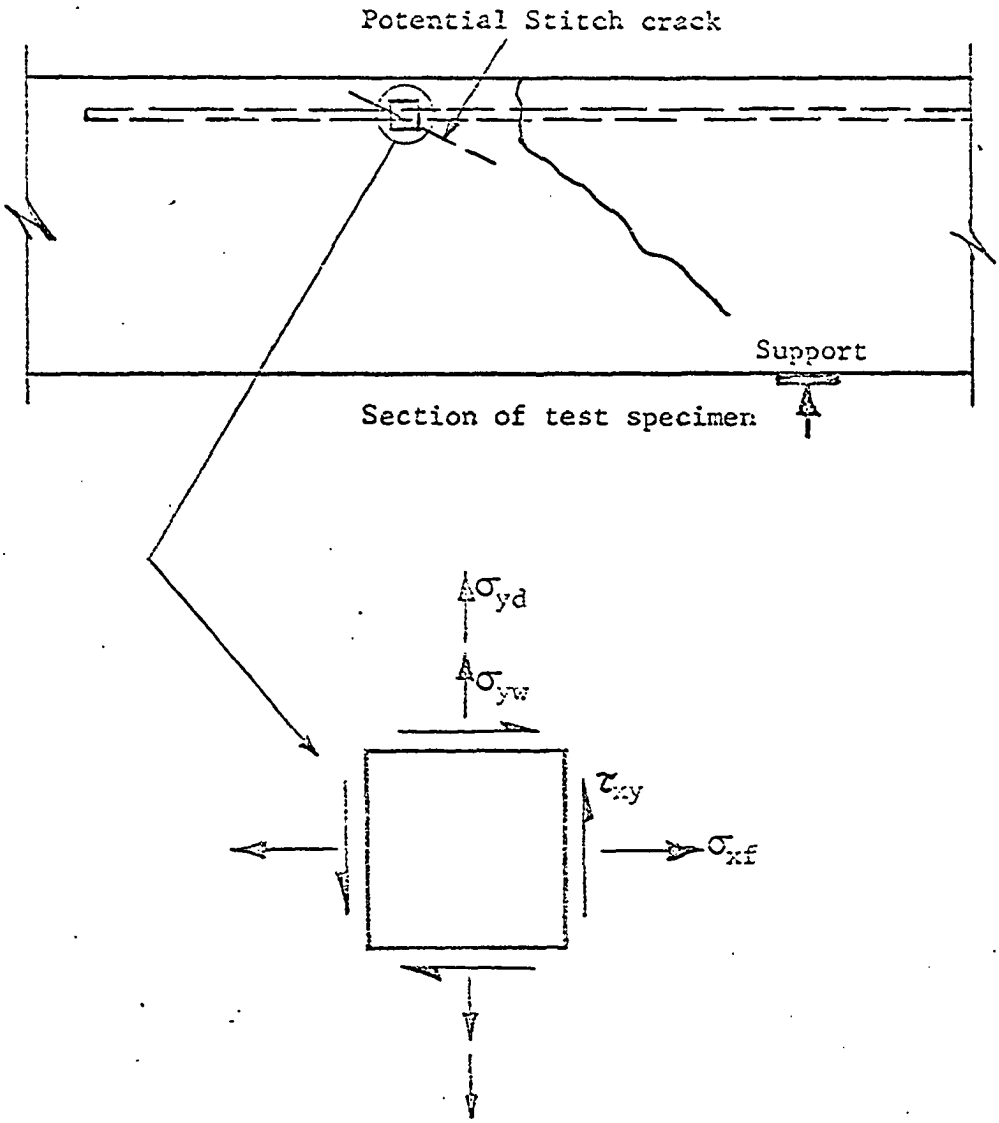

Stresses on element adjacent to reinforcement

Fig. 13. Stresses causing stitch cracking

$$\sigma_{xf} = \text{constant} \cdot \frac{f_s}{n} \qquad \text{where } n = \frac{E_s}{E_c}$$

$$\sigma_{xf} = K_1 \frac{f_s}{n}$$

The shearing stress, τ_{xy}, in the concrete was assumed proportional to the average shearing stress on the total cross section.

$$\tau_{xy} = \text{constant} \cdot \frac{V}{bd}$$

$$\tau_{xy} = K_2 \frac{V}{bd}$$

The vertical normal stress, σ_y, at a point adjacent to the reinforcing steel was assumed to be composed of stress components due to wedging plus those due to doweling. The stress component due to wedging, σ_{yw}, was assumed to be proportional to the maximum tangential stress in the concrete at the interface of the concrete and steel induced by the normal radial component of bond stress, f. The effect of f acting in planes perpendicular to the longitudinal axis of the reinforcing bars was subject to a photoelasticity analysis (Appendix B). In particular, the maximum tangential stress concentration ratio, G, was determined at the boundary of the holes made by reinforcing bars as a function of bar spacing using a plane stress case.

$$G = \frac{\sigma_1}{f}$$

and

$$\sigma_{yw} = \text{constant} \cdot Gf$$

The values of G for various clear bar spacing are plotted in Fig. 14. The following relationship was assumed to exist between f and u (Fig. 1):

$$f = u \tan \phi$$

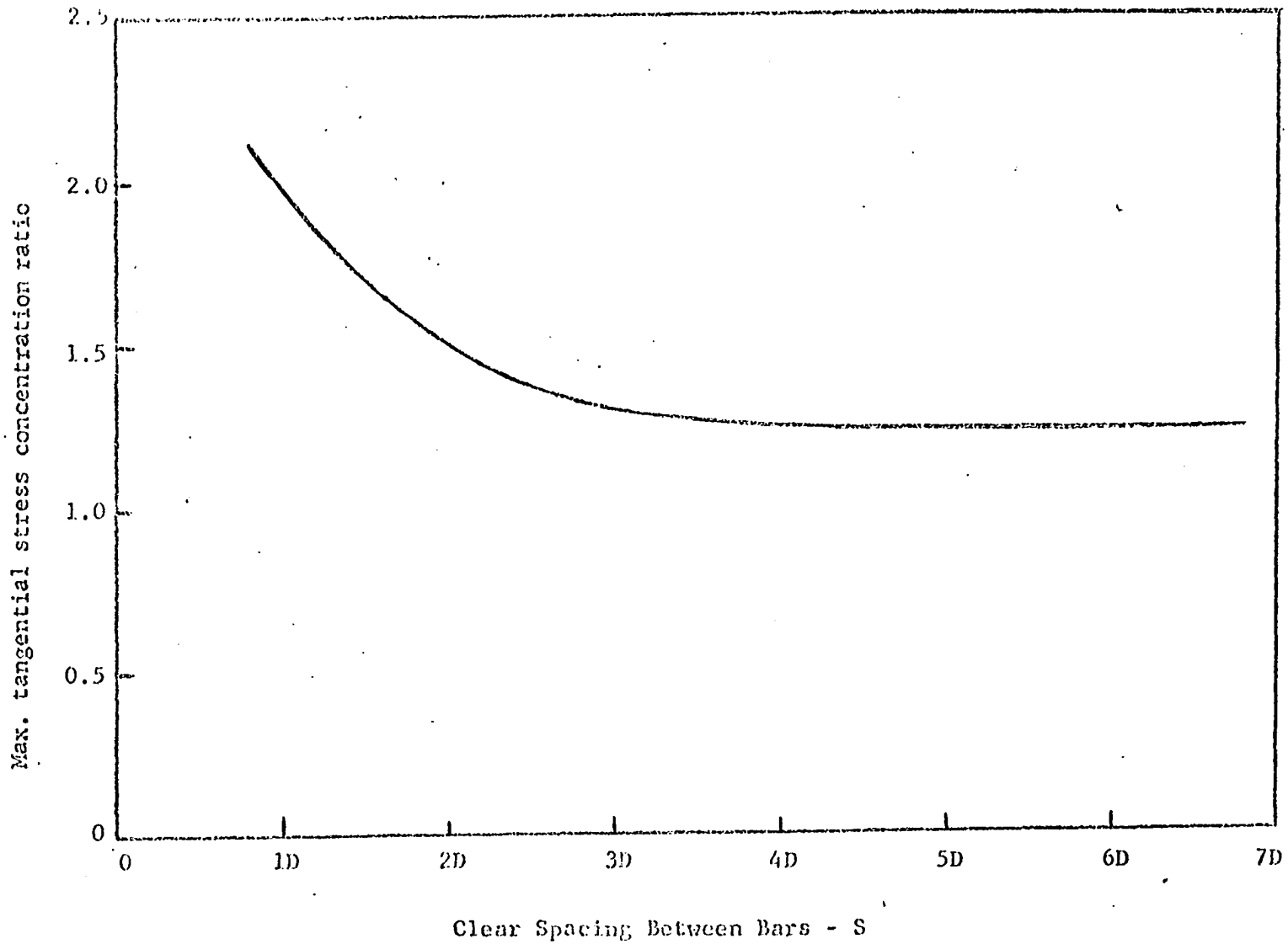

Fig. 14. Maximum tangential stress concentration ratio versus clear bar spacing

so

$$\sigma_{yw} = K_3 Gu$$

The second component of the vertical stress, σ_{yd}, is the stress due to doweling forces which was assumed to be a function of the area of steel in the cross section. Adding these two σ_y components yields:

$$\sigma_y = \sigma_{yw} + \sigma_{yd}$$

$$\sigma_y = K_3 Gu + K_4 A_s$$

When the maximum normal principle stress, σ_{max}, equals the tensile strength of concrete, f'_t, anchorage failure is pending. The tensile strength of concrete is assumed to be proportional to the square root of compressive strength of the concrete. Thus,

$$\sigma_{max} = f'_t = \text{constant} \cdot \sqrt{f'_c}$$

or

$$\sigma_{max} = K_5 \sqrt{f'_c}$$

Substituting the above stress values into the principle stress equation yields:

$$2K_5 \sqrt{f'_c} = K_1 \frac{f_s}{n} + K_3 Gu + K_4 A_s + \sqrt{\left[K_1 \frac{f_s}{n} - K_3 Gu - K_4 A_s\right]^2 + \left[2K_2 \frac{V}{bd}\right]^2}$$

Since,

$$u = \frac{f_s D}{4L''}$$

and

$$f_s = \frac{M}{A_s jd}$$

the principle stress equation reduces to

$$2K_5\sqrt{f'_c} = \frac{M}{A_s jd}\left[\frac{K_1}{n} + \frac{K_3 GD}{4L''}\right] + K_4 A_s + \sqrt{\left[\frac{M}{A_s jd}\left[\frac{K_1}{n} - \frac{K_3 GD}{4L''}\right] - K_4 A_s\right]^2 + \left[2K_2 \frac{V}{bd}\right]^2}$$

By rearrangement and bringing $\frac{V}{bd}$ to the left side of the equation and substituting p for $\frac{A_s}{bd}$, the equation becomes

$$\frac{V}{2bdK_5\sqrt{f'_c}} = \frac{1}{\frac{M}{Vpjd}\left[\frac{K_1}{n} + \frac{K_3 GD}{4L''}\right] + \frac{K_4 A_s bd}{V} + \sqrt{\left[\frac{M}{Vpjd}\left[\frac{K_1}{n} - \frac{K_3 GD}{4L''}\right] - \frac{K_4 A_s bd}{V}\right]^2 + (2K_2)^2}}$$

Further simplification can be made by replacement of the term, $n = \frac{E_s}{E_c}$. The modulus of elasticity of steel, E_s, is a constant. The modulus of elasticity of concrete, E_c, may be expressed approximately as a function of $\sqrt{f'_c}$, so that E_c equals a constant time $\sqrt{f'_c}$. Therefore, 1/n can be expressed as a constant times $\sqrt{f'_c}$ and the expression becomes

$$\frac{V}{2bdK_5\sqrt{f'_c}} = \frac{1}{\frac{M}{Vpd}\left[K_6\sqrt{f'_c} + \frac{K_3 GD}{4L''}\right] + \frac{K_4 bdA_s}{V} +}$$

$$+ \sqrt{\left[\frac{M}{Vpd}\left[K_6\sqrt{f'_c} - \frac{K_3 GD}{4L''}\right] - \frac{K_4 bdA_s}{V}\right]^2 + (2K_2)^2}$$

where K_6 is a new constant.

The above expression gave the parameters to be investigated and they were considered in the following form:

$$\frac{V}{bd\sqrt{f'_c}} = \frac{1}{\frac{M}{Vpd}\left[K_7\sqrt{f'_c} + K_8\frac{GD}{L''}\right] + \frac{K_9 bdA_s}{V} + K_{10}}$$

The relationship indicates the following with regard to the ultimate shear capacity as a result of an anchorage failure:

$$\text{since } v = \frac{V}{bd}$$

v increases with increasing concrete strength.

v decreases with increasing M/V.

v increases with increasing embedment length.

v decreases with increasing bar diameter.

v decreases with A_s in one term and is increased in another by the value of p.

Calculating the ultimate shear capacity as limited by the anchorage strength may appear misleading, however, the ultimate shear capacity can be related to the anchorage strength as follows if desired:

$$u = \frac{V \quad L'}{\Sigma o j d \cdot L''}$$

Where L' equals L'' minus the extension beyond countraflexure point. However, it is not necessary to calculate the unit bond stress in flexural members since the derived expression can be used as an additional limit placed on the ultimate design shear stress.

Evaluation of K's

Values of the K's in the above relationship cannot be determined accurately without a considerable amount of data; however, relative orders of magnitudes were easily determined with the use of the available data from this investigation.

The experimental numerical values of the four parameters,

$$\frac{V}{bd\sqrt{f'_c}}, \quad \frac{M\sqrt{f'_c}}{Vpd}, \quad \frac{MGD}{VpdL''}, \text{ and } \frac{bdA_s}{V},$$

are listed in Table 9 of Appendix A. Using the above as data, a multiple linear regression of $\frac{V}{bd\sqrt{f'_c}}$ was performed in order to determine a fitted curve for it using the other three parameters as independant variables. A standard computer program for statistical and numerical analysis, OMNITAB, which was prepared by the Statistics Department of Iowa State University for the IBM 360/65 computer, was utilized in the fitting of the curve and obtaining the values for the K's (2). The values of K_7, K_8, K_9, and K_{10} were obtained by regression to be as follows:

$$K_7 = 3.15 \times 10^{-6}$$

$$K_8 = 8.87 \times 10^{-3}$$

$$K_9 = 6.62$$

$$K_{10} = 0.023$$

Substituting the above values into the expression for the ultimate shear stress and transposing like terms to the left side of the expression, the following relationship can be determined:

$$\frac{V}{bd} = \frac{1000\left[\sqrt{f'_c} - 6.62\ A_s\right]}{\frac{M}{Vpd}\left[\frac{\sqrt{f'_c}}{316} + \frac{8.87GD}{L''}\right] + 23}$$

Comparison was made between the fitted values of $\frac{V}{bd\sqrt{f'_c}}$ and the experimental values with the plot in Fig. 15. The maximum error from the fitted curve is approximately 11 percent.

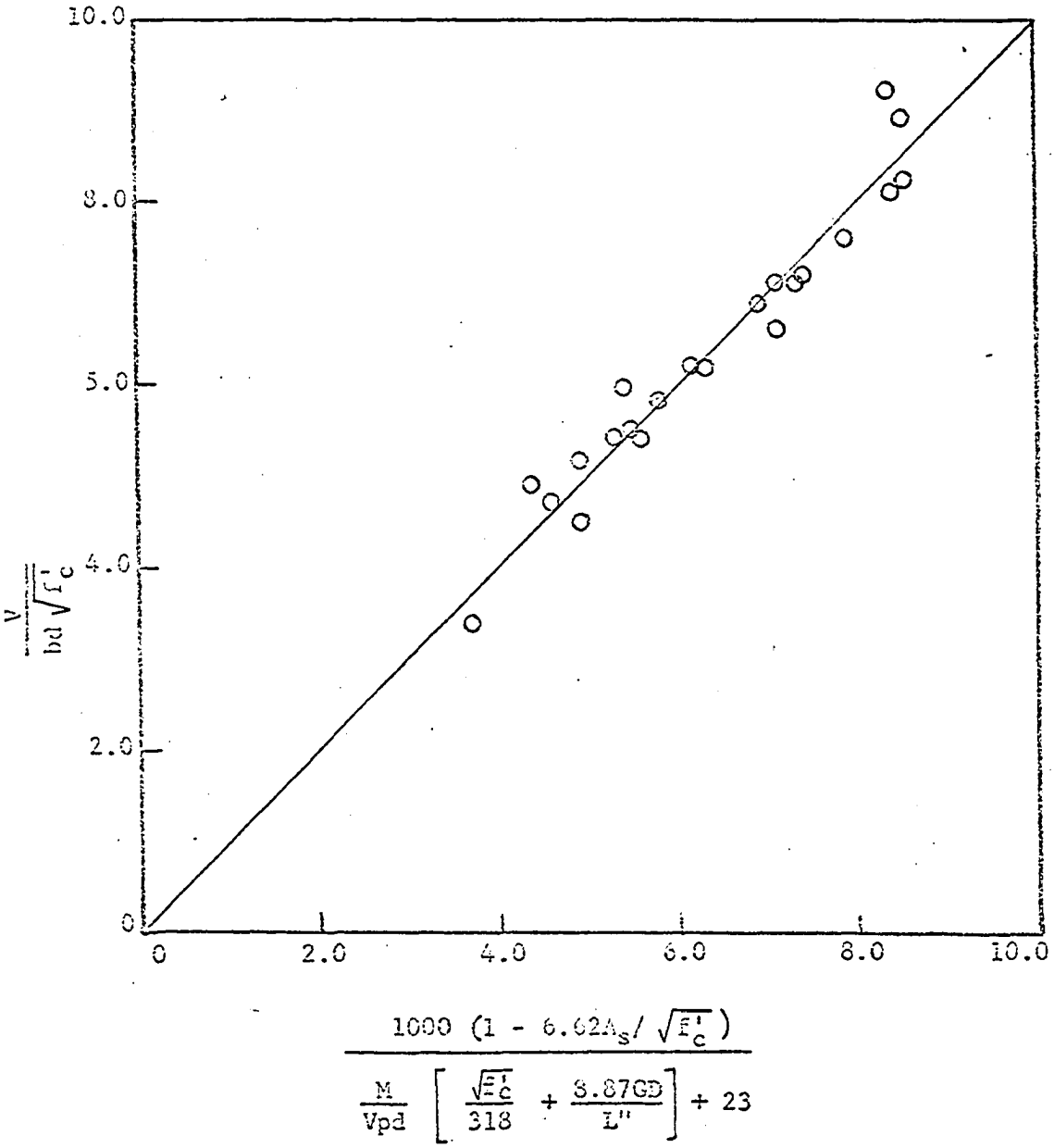

Fig. 15. Experimental $\frac{V}{bd\sqrt{f'_c}}$ versus derived value - top bars

Bottom bars

As was pointed out earlier, bond strength of bottom bars is higher than that of top bars. Assuming this to be mainly as a result of increased tensile strength between bottom and top cast concrete, the terms in the ultimate shear equation containing $\sqrt{f'_c}$ were multiplied by 1.16 to obtain an expression governing an anchorage failure for bottom bars.

$$\frac{V}{bd} = \frac{1000 \left[\sqrt{f'_c} + 5.71 A_s \right]}{\frac{M}{Vpd} \left[\frac{\sqrt{f'_c}}{318} + \frac{7.65GD}{L''} \right] + 20}$$

The experimental values of $V/bd \sqrt{f'_c}$ from the five bottom bar tests can be compared to the derived values obtained from the above expression by using the plot shown in Fig. 16. The experimental values are all within 12 percent of the $V/bd\sqrt{f'_c}$ values obtained from the derived expression.

University of Texas data

To check the validity of the derived equation for ultimate anchorage failure, the value of $V/bd\sqrt{f'_c}$ from the bottom bar equation was compared with experimental values from beam tests conducted at the University of Texas (7). The data from the Texas tests were obtained from the same type of beam specimen used in this study. The test beams utilized No. 7 and No. 11 bars, both with and without stirrups. The experimental values of $V/bd\sqrt{f'_c}$ from the Texas studies were compared with the derived values in the plot in Fig. 17.

Appropriate symbols are shown on the plot to identify size and number of longitudinal reinforcing bars and the amount of shear reinforcement. The

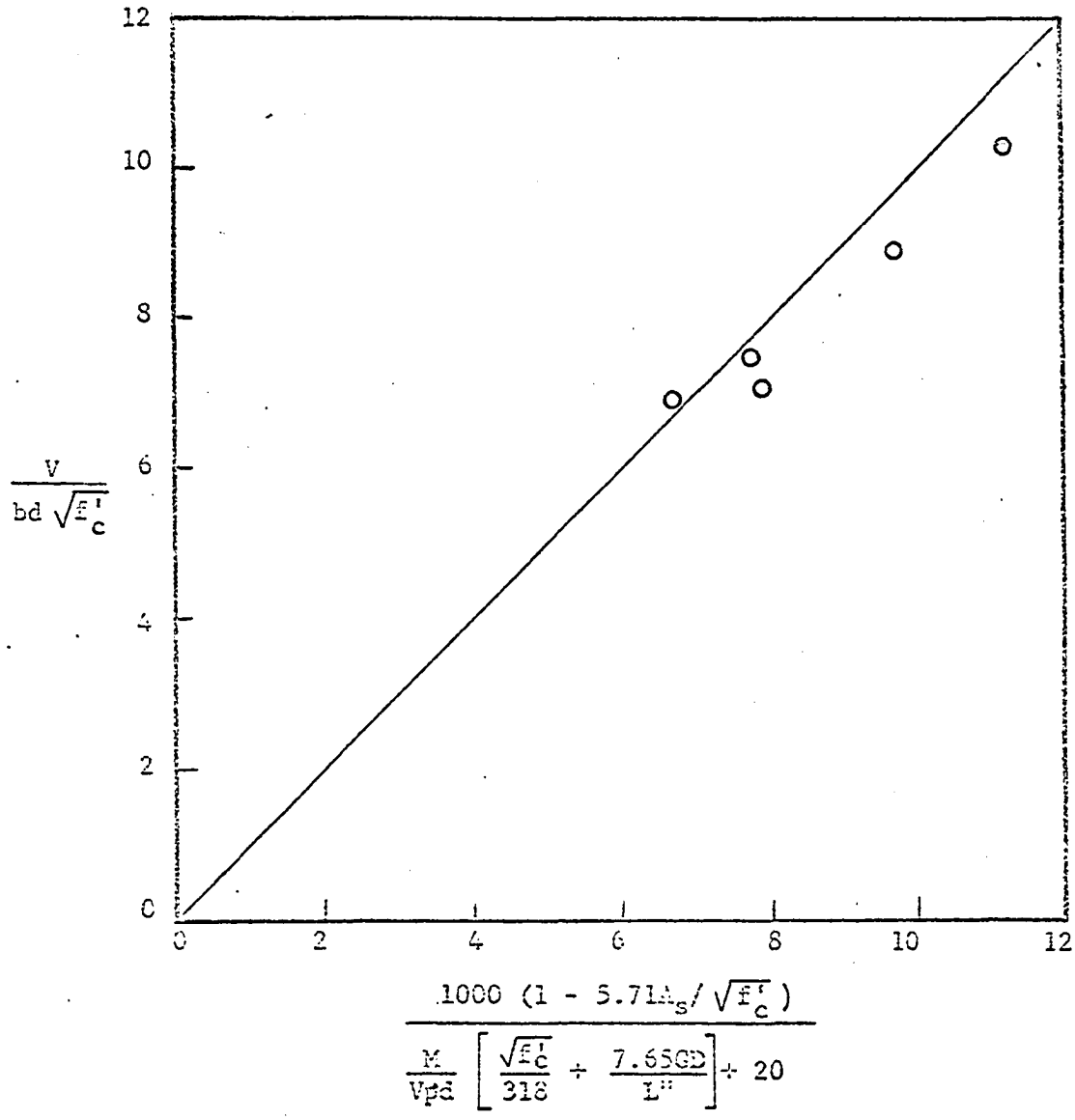

Fig. 16. Experimental $\frac{V}{bd\sqrt{f'_c}}$ versus derived value - bottom bars

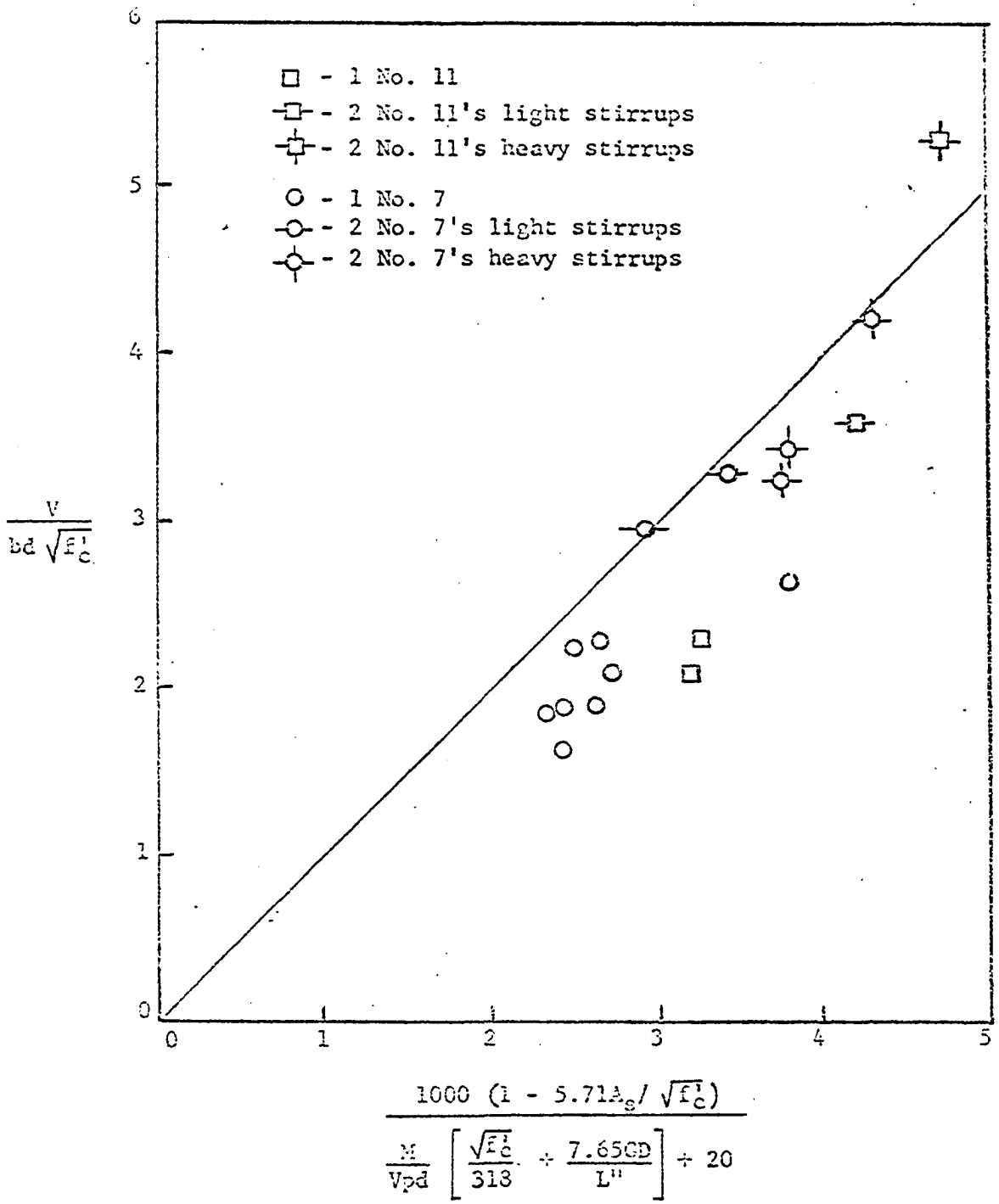

Fig. 17. Experimental $\frac{V}{bd\sqrt{f'_c}}$ versus derived value for bottom bars - University of Texas data

term "light stirrups" was defined to be an amount of shear reinforcement such that $rf_v = 0.01f'_c$ and "heavy stirrups" refer to $rf_v = 0.05f'_c$.

Although there is good agreement in some cases, there is also as much as 30 percent difference at times. However, several different variables were involved with the Texas tests. Most of the beams had no extension beyond the point of countraflexure. The amount of shear reinforcement is also a major variable, with many tests employing none at all. In addition, the amount of concrete cover varied from 0.9 to 3.1D. In the shear equation, a value of G equal to 1.25 was used in all cases.

In general, the ultimate shear at bond failure in the beams with no stirrups and one longitudinal test bar was 20 to 30 percent below the values predicted by the derived equation. However, it must be pointed out that the bond failures in specimens with one bar are different from those of 2 or more bars (4, 15). The failures are mainly ones of splitting and they lack the formation of the short diagonal or stitch cracks. The failures of these specimens occurred at a low shear stress near the value of the concrete shear strength, $2\sqrt{f'_c}$. Modifications of the values of the K's could have been made in order that a curve could have been fitted to account for single bars, but this was not done since single bars in beams very seldom appear in design.

The ultimate shear at bond failure in the beam specimens with shear reinforcement and two bars agreed quite well with those values obtained from the derived equation. Deviations of experimental values were in the order of 13 percent of the derived $V/bd\sqrt{f'_c}$.

SUMMARY AND CONCLUSIONS

The object of this investigation was to study the effect of bar spacing, beam width, and number of longitudinal bars on the ultimate anchorage bond capacity of reinforced concrete beams. The objectives were accomplished by analysis of experimental test results and development of a semi-rational ultimate shear equation.

A total of 27 beams consisting of 22 top bar specimens and 5 bottom bar specimens were tested. A simply supported test beam with one end cantilevered was employed, simulating a continuous structure. The number of test bars per beam varied from 2 to 7 and the beam widths were 12, 16, 18 and 24 inches. The following observations are noted:

1. Although bond strength is defined as the maximum force per unit surface area of reinforcement, it appears not to be a matter of amount of stress that the surface between the concrete and steel can sustain, but the maximum tensile stress the concrete surrounding the reinforcement can withstand. All failures observed in this investigation involved a tensile failure in the concrete.
2. Within each beam width tested, bond strength was consistently increased as the bar spacing and the ratio b/N was increased. Bond was only slightly increased by increased beam width. It was found that increased embedment length increased the ultimate unit anchorage stress which was contrary to previous research findings. The anchorage capacity consistently decreased as the number of bars per beam increased. ACI Code design allowables were insufficient for the 18 and 24 inch width beams with top bars of 5 or more. In

addition, in two of the 12 and 18 inch width beams, the ACI Code allowables were found to be more than 100 percent conservative.

3. Stirrups, which were used mainly to avoid shear failures, were observed to arrest crack propagation and give the beams more ductility after ultimate load. However, a variation of stirrup size or shear capacity did not substantially affect the ultimate anchorage capacity.
4. Failure patterns of top and bottom bars were similar. Two types of cracks developed besides the usually flexural and major diagonal cracks. Short diagonal or stitch cracks formed on oblique planes through the reinforcement and longitudinal splitting occurred through the concrete cover running parallel to the longitudinal reinforcement. The anchorage strength of bottom bars was 1.12 times that obtained for top cast bars. This appeared to be mainly as a result of change in concrete tensile strength between bottom and top cast concrete.
5. For top bar tests, a variation of nearly 360 percent was obtained between the maximum anchorage bond, 691 psi, and the lowest, 189 psi.

Using the experimental results, an expression was derived based on ultimate anchorage capacity. Considering redistribution of stresses due to diagonal cracking, the steel stress that can be developed at the maximum moment at the support is:

$$\text{Top bars;}\quad f_s = \frac{1}{A_s}\left[110(L'' - d)\sqrt{f'_c} + \frac{1}{2}(V_{ult} - V_c)\right]$$

$$\text{Bottom bars;}\quad f_s = \frac{1}{A_s}\left[128(L'' - d)\sqrt{f'_c} + \frac{1}{2}(V_{ult} - V_c)\right]$$

Another semirational expression was derived, limiting the ultimate shear capacity of the beams. The derivation was based upon a principal stress approach. Stresses due to wedging, doweling, flexure, and shear were considered. Parameters were obtained, and the following expressions were determined by a multiple regression analysis:

$$\text{Top bars;}\quad \frac{V}{bd} = \frac{1000\,(\sqrt{f'_c} - 6.62A_s)}{\frac{M}{Vpd}\left[\frac{\sqrt{f'_c}}{318} + \frac{8.87GD}{L''}\right] + 23}$$

$$\text{Bottom bars;}\quad \frac{V}{bd} = \frac{1000\,(\sqrt{f'_c} - 5.71A_s)}{\frac{M}{Vpd}\left[\frac{\sqrt{f'_c}}{318} + \frac{7.65GD}{L''}\right] + 20}$$

The value of G, the maximum tangential stress concentration ratio, was obtained by a photoelastic analysis of models of the specimens' cross sections. The factor G for each bar spacing was taken from the plot shown in Fig. 14.

Future studies should consider the effect of depth, d, bar diameter D, extensions beyond moment inflection, and the amount and arrangement of shear reinforcement.

ACKNOWLEDGEMENTS

This investigation was conducted in the Structural Research Laboratory of the Engineering Research Institute at Iowa State University with the aid of Engineering Research Institute research funds.

The investigation was under the general guidance of Dr. R. E. Untrauer, Professor of Civil Engineering and Director of the Structural Research Laboratory. The author wishes to express his appreciation to Dr. Untrauer for his advice and guidance throughout the investigation.

Special thanks are due Professor William F. Riley of the Engineering Mechanics Department. The author is grateful for his help in the planning and preparation of the photoelastic study.

The use of the metal forms from Economy Forms Corporation of Des Moines, Iowa, is acknowledged. The assistance of fellow graduate students, Messrs. Arendts, Chinnen, Kao, Porter, Schauer, Schuster, Watanabe, and Wilson is also acknowledged in the casting and testing of the specimens.

LITERATURE CITED

1. American Concrete Institute. ACI standard building code requirements for reinforced concrete. Detroit, Michigan, American Concrete Institute. 1963.

2. Chamberlain, R. L. and Jowett, D. The omnitab programming system, a guide for users. Houston, Tex., Houston Data Service Center, Shell Oil Co. 1968.

3. Chamberlin, S. J. Spacing of reinforcement in beams. American Concrete Institute Journal 28: 113-134. 1956.

4. Committee 408 on Bond. Bond stress: the state of the art. American Concrete Institute Journal 63: 1161-1190. 1966.

5. Dally, James W. and Riley, William F. Experimental stress analysis. 1st ed. New York, N.Y., McGraw-Hill Book Co., Inc. 1965.

6. Durelli, A. J. and Riley, W. F. Introduction to photomechanics. 1st ed. Englewood Cliffs, N.J., Prentice-Hall, Inc. 1965.

7. Ferguson, P. M. and Thompson, J. N. Development length of high strength reinforcing bars in bond. American Concrete Institute Journal 59: 887-992. 1962.

8. Ferguson, P. M. and Thompson, J. N. Development length of large high strength reinforcing bars in bond. American Concrete Institute Journal 62: 71-93. 1965.

9. Ferguson, P. M., Turpin, R. D., and Thompson, J. N. Minimum bar spacing as a function of bond and shear strength. American Concrete Institute Journal 25: 869-887. 1954.

10. Harris, John F. The influence of applied normal pressure on bond between concrete and reinforcing steel in pull-out tests. Unpublished M.S. thesis. Ames, Iowa, Library, Iowa State University of Science and Technology. 1964.

11. Henry, Robert L. The effect of normal pressure on bond between reinforcing steel and concrete. Unpublished M.S. thesis. Ames, Iowa Library, Iowa State University of Science and Technology. 1963.

12. Mathey, Robert C. and Watstein, David. Investigation of bond in beam and pull-out specimens with high-yield-strength deformed bars. American Concrete Institute Journal 32: 1071-1090. 1961.

13. McWilliams, Conrad A. Influence of stirrup confinement on bond strength of concrete. Unpublished M.S. thesis. Ames, Iowa, Library, Iowa State University of Science and Technology. 1965.

14. Robinson, J. R. Influence of transverse reinforcement on shear and bond strength. American Concrete Institute Journal 62: 343-362. 1965.

15. Warren, George E. Effect of bar spacing on bond strength. Unpublished M.S. thesis. Ames, Iowa, Library, Iowa State University of Science and Technology. 1967.

APPENDIX A

Table 1 Reinforcing steel strength

Specimen	Longitudinal Steel f_y ksi	Longitudinal Steel f_u ksi	Stirrup Steel f_y ksi	Stirrup Steel f_u ksi
2A46V	74.4	117.0	47.1	80.0
3A46V	83.0	116.3	56.4	87.1
4A46V	74.4	117.0	47.1	80.0
3B46W	83.0	116.3	56.0	87.0
3B38W	83.0	116.3	56.0	87.0
2C46V	74.7	117.0	46.1	74.7
3C46V	83.0	116.3	56.4	87.1
4C46V	74.7	105.3	46.1	74.7
5C46V	83.0	116.3	46.1	74.7
6C46V	74.7	105.3	46.1	74.7
3D46V	90.0	117.4	56.8	91.7
4D46V	83.0	116.3	47.1	80.0
5D46V	74.4	117.0	46.2	75.5
6D46V	74.4	117.0	46.2	75.5
7D46V	74.4	117.0	46.2	75.5
5C36V	74.3	105.9	57.7	92.0
5C62V	74.3	105.9	46.8	73.6
5C76V	85.0	106.0	46.8	73.6
2C35V	90.0	106.0	57.7	92.0
3C35X	90.0	117.4	57.7	92.0
5C46Y	74.7	117.0	44.0	70.7
5C76Z	85.0	117.4	46.0	76.0
5C46V*	74.7	117.4	57.4	97.0
4C46V*	90.0	117.0	57.4	97.0
5C62V*	90.0	117.0	57.4	97.0
3C35X*	90.0	117.0	57.4	97.0
2A35V*	90.0	117.0	57.4	97.0

Table 2 Specimen concrete properties

Specimen	Slump inches	Compressive Strength f'_c psi	Splitting Tensile Strength f'_t psi	Adjustment Factor $\sqrt{\frac{4000}{f'_c}}$	$\sqrt{f'_c}$	$\frac{f'_t}{\sqrt{f'_c}}$
2A46V	3 1/2	3170	373	1.125	56.3	6.63
3A46V	3 1/2	3370	440	1.091	58.1	7.57
4A46V	4 1/2	3720	441	1.038	61.0	7.23
3B46W	3	3180	392	1.122	56.4	6.96
3B38W	3	3090	348	1.136	55.6	6.26
2C46V	2 1/2	3510	511	1.067	59.3	8.61
3C46V	2 1/2	4200	449	0.977	64.8	6.94
4C46V	2 1/2	3860	464	1.017	62.1	7.46
5C46V	2	4300	456	0.964	65.6	6.96
6C46V	2 1/2	3410	440	1.083	58.4	7.54
3D46V	2 1/2	3610	458	1.053	60.1	7.61
4D46V	2 1/2	3950	445	1.008	62.9	7.08
5D46V	4	3850	468	1.022	62.1	7.52
6D46V	4	3410	391	1.074	58.4	6.70
7D46V	2 1/2	3710	405	1.039	60.9	6.65
5C36V	3 1/2	4110	407	0.987	64.1	6.34
5C62V	3 1/2	4190	429	0.978	64.7	6.63
5C76V	3 1/2	4360	452	0.957	66.1	6.84
2C35V	3 1/2	3860	471	1.019	62.1	7.58
3C35X	3 1/2	3850	431	1.019	62.1	6.94
5C46Y	4 1/2	3800	430	1.026	61.6	6.98
5C76Z	4 1/2	3940	457	1.008	62.8	7.28
5C46V*	3	3990	445	1.001	63.2	7.04
4C46V*	3	3840	436	1.022	62.0	7.03
5C62V*	3	3950	441	1.007	62.9	7.01
3C35X*	3	3270	386	1.106	57.2	6.74
2A35V*	3	3690	440	1.041	60.8	7.24

Table 3 Dimensions for variation of load arrangement (Fig. 2)

Specimen	Embedment Length inches	c inches	g inches	m inches	o inches	t inches	z inches	Total Beam Length
2A46V	46	8	55 1/4	65 1/2	55 1/4	8	88	16'-0"
3A46V	46	8	55 1/4	65 1/2	55 1/4	8	88	16'-0"
4A46V	46	8	55 1/4	65 1/2	55 1/4	8	88	16'-0"
3B46W	46	8	54 1/2	67	54 1/2	8	88	16'-0"
3B38W	38	8	62	52	62	8	88	16'-0"
2C46V	46	8	55 1/4	65 1/2	55 1/4	8	88	16'-0"
3C46V	46	8	55 1/4	65 1/2	55 1/4	8	88	16'-0"
4C46V	46	8	55 1/4	65 1/2	55 1/4	8	88	16'-0"
5C46V	46	8	55 1/4	65 1/2	55 1/4	8	88	16'-0"
6C46V	46	8	55 1/4	65 1/2	55 1/4	8	88	16'-0"
3D46V	46	5	50	60	72	5	102	16'-0"
4D46V	46	8	55 1/4	65 1/2	55 1/4	8	88	16'-0"
5D46V	46	5	50	60	72	5	102	16'-0"
6D46V	46	5	50	60	72	5	102	16'-0"
7D46V	46	5	50	60	72	5	102	16'-0"
5C36V	36	8	64	50	41	5	65 9/16	14'-0"
5C62V	62	6	81	76	70	7	95 7/8	20'-0"
5C76V	76	5	59	90	57	29	83 15/16	20'-0"
2C35V	35	7	64	50	42	5	67 11/16	14'-0"
3C35X	35	7	64	50	42	5	67 11/16	14'-0"
5C46Y	46	5	65	60	56	6	82 1/4	16'-0"
5C76Z	76	8	67 1/4	90	57	17 3/4	83 7/16	20'-0"
5C46V*	46	8 3/4	44	60	52	6 1/4	86 1/8	14'-3"
4C46V*	46	8 3/4	46	60	52	6 1/4	86 1/8	14'-3"
5C62V*	62	5 1/2	72	76	72	14 1/2	120 3/4	20'-0"
3C35X*	35	6 1/4	42	50	64	5 3/4	88 1/4	14'-0"
2A35V*	35	6 1/4	42	50	64	5 3/4	88 1/4	14'-0"

Table 4 Specimen cross section properties

Specimen	b in.	d in.	Clear Longitudinal bar Spacing in.	Total Depth in.
2A46V	12	17.3	5.5	20
3A46V	12	17.3	2.2	20
4A46V	12	17.3	1.1	20
3B46W	16	16.8	4.8	19.5
3B38W	16	16.8	4.8	19.5
2C46V	18	17.3	11.5	20
3C46V	18	17.3	5.2	20
4C46V	18	17.3	3.1	20
5C46V	18	17.3	2.0	20
6C46V	18	17.3	1.4	20
3D46V	24	17.3	8.2	20
4D46V	24	17.3	5.1	20
5D46V	24	17.3	3.5	20
6D46V	24	17.3	2.6	20
7D46V	24	17.3	2.0	20
5C36V	18	17.3	2.0	20
5C62V	18	17.3	2.0	20
5C76V	18	17.3	2.0	20
2C35V	18	17.3	11.5	20
3C35X	18	17.3	5.2	20
5C46Y	18	17.3	2.0	20
5C76Z	18	17.3	2.0	20
5C46V*	18	17.3	2.0	20
4C46V*	18	17.3	3.1	20
5C62V*	18	17.3	2.0	20
3C35X*	18	17.3	5.2	20
2A35V*	12	17.3	5.5	20

Number of Longitudinal Bars	Percent Steel P %	Stirrup Size No.	Stirrup Spacing in.	Web Reinforcing Ratio r
2	0.96	5	5	0.1033
3	1.44	5	5	0.1033
4	1.93	5	5	0.1033
3	1.15	5	5.5	0.0705
3	1.15	5	5.5	0.0705
2	0.64	5	5	0.0689
3	0.96	5	5	0.0689
4	1.28	5	5	0.0689
5	1.60	5	5	0.0689
6	1.93	5	5	0.0689
3	0.72	5	5	0.0517
4	0.96	5	5	0.0517
5	1.20	5	5	0.0517
6	1.44	5	5	0.0517
7	1.69	5	5	0.0517
5	1.60	5	5	0.0689
5	1.60	5	5	0.0689
5	1.60	5	5	0.0689
2	0.64	5	5	0.0689
3	0.96	5	4	0.0862
5	1.60	6	5	0.0978
5	1.60	4	5	0.0444
5	1.60	5	5	0.0689
5	1.28	5	5	0.0689
5	1.60	5	5	0.0689
3	0.96	5	4	0.0862
2	0.96	5	5	0.1033

Table 5 Measured and computed experimental data

Specimen	Ultimate Machine Load Kips	Shear Kips	Average Shear Stress psi	Ultimate Moment in·Kips	Steel Stress ksi	Adjusted Steel Stress ksi
2A46V	195	89	430	2660	92.2	103.6
3A46V	236	108	521	3200	76.5	83.5
4A46V	255	117	563	3450	61.4	64.7
3B46W	241	108	439	3240	73.7	82.7
3B38W	222	121	491	2740	60.0	68.2
2C46V	237	108	347	3240	105.6	112.0
3C46V	303	139	446	4100	90.0	87.9
4C46V	299	137	439	4050	67.5	68.7
5C46V	277	127	407	3760	48.7	47.0
6C46V	235	108	346	3210	35.0	37.9
3D46V	275	138	333	4140	89.2	94.0
4D46V	306	141	340	4160	66.6	67.2
5D46V	230	115	277	3500	46.0	47.0
6D46V	166	83	201	2580	28.6	30.8
7D46V	245	123	297	3710	35.5	36.9
5C36V	261	132	424	2540	31.8	31.3
5C62V	220	108	347	4960	68.2	66.7
5C76V	272	106	341	6400	92.5	94.3
2C35V	272	139	447	2530	79.1	80.6
3C35X	312	160	514	2890	61.2	58.6
5C46Y	239	119	382	3540	46.2	47.4
5C76Z	231	92	286	5560	79.4	80.1
5C46V*	333	147	472	4220	56.4	56.5
4C46V*	308	136	437	3910	64.6	66.1
5C62V*	276	135	433	6020	88.2	88.9
3C35X*	310	158	508	2820	60.7	67.1
2B35V*	254	130	626	2300	75.4	78.5

Bond Stress psi	Adjusted Bond Stress psi	Stitch Cracks Began $\%P_{ult}$	Cracking to inflection Point $\%P_{ult}$	Mode of Failure
576	649	72	86	Crushing-bond
459	501	61	79	Bond
376	391			Bond
452	508			Bond
446	506			Bond
647	691			Crushing-bond
552	539			Bond
414	421	77	93	Bond
299	288			Bond
215	233	97	98	Bond
547	576	97	97	Bond
408	411			Bond
282	288	100	100	Bond
176	189	100	100	Bond
218	227	94	94	Bond
250	246	82	89	Bond
311	304	79	98	Bond
343	328	79	81	Bond
638	650	86	87	Bond
493	502	65	86	Bond
284	291	84	97	Bond
295	297	67	100	Bond
346	347	86	98	Bond
397	405	70	92	Bond
402	404	83	99	Crushing-bond
490	542	63	83	Crushing-bond
609	634	61	100	Crushing-bond

Table 6 Comparison of experimental results with ACI Code allowables

Specimen	Ultimate Shear V_{ult} kips	Ultimate Bond Strength u_{ult} psi	$\sqrt{f'_c}$	Concrete Shear V_c kips	Allowable Shear V_{code} kips
2A46V	89	566	56.3	27	128
3A46V	108	459	58.1	30	151
4A46V	117	376	61.0	34	135
3B46W	108	452	56.4	37	146
3B38W	121	446	55.6	37	146
2C46V	108	647	59.3	40	139
3C46V	139	552	64.8	46	167
4C46V	137	414	62.1	47	146
5C46V	127	299	65.6	51	150
6C46V	108	215	58.4	50	149
3D46V	138	547	60.1	55	177
4D46V	141	408	62.9	60	161
5D46V	115	270	62.1	61	160
6D46V	83	163	58.4	61	160
7D46V	123	207	60.9	66	165
5C36V	132	250	64.1	50	174
5C62V	108	311	64.7	46	146
2C35V	139	638	62.1	42	166
3C35X	160	493	62.1	44	198
5C76V	106	343	66.1	44	144
5C46Y	119	284	61.6	49	183
5C76Z	92	295	62.8	42	106
5C46V*	147	346	63.2	50	173
4C46V*	136	397	62.0	47	170
5C62V*	135	402	62.9	45	168
3C35X*	158	490	57.2	41	195
2A35V*	130	606	60.8	29	152

Allowable Bottom Bar Bond u_B psi	Allowable Top Bar Bond u_T psi	$\frac{V_{ult}}{V_{code}}$	$\frac{u_{ult}}{u_B}$	$\frac{u_{ult}}{u_T}$
379	268	0.71	1.49	2.11
383	276	0.72	1.20	1.66
419	290	0.87	0.90	1.30
380	268	0.74	1.19	1.69
374	364	0.83	1.19	1.69
402	283	0.78	1.61	2.29
437	308	0.83	1.79	1.79
418	295	0.94	1.40	1.40
442	312	0.85	0.96	1.08
393	277	0.73	0.55	0.77
404	285	0.78	1.35	1.92
424	299	0.88	0.96	1.36
418	295	0.72	0.65	0.91
393	281	0.52	0.41	0.58
411	290	0.75	0.50	0.71
432	305	0.76	0.58	0.82
437	308	0.74	0.71	1.01
418	295	0.84	1.53	2.16
418	295	0.81	1.18	1.67
446	315	0.73	0.77	1.09
415	293	0.65	0.68	0.97
424	299	0.87	0.70	0.99
426	300	0.85	0.81	1.15
418	295	0.80	0.95	1.34
424	299	0.80	0.95	1.34
385	272	0.81	1.27	1.74
410	289	0.86	1.48	2.10

Table 7 Effect of redistribution

Specimen	Ultimate Shear V_{ult} kips	Concrete Shear V_c kips	$\frac{A_v f_{yd}}{s}$ kips	Steel Stress f_{sr} ksi	Bond Stress u_{ur} psi	Adjusted Steel Stress f_{sr}	Adjusted Bond Stress u_{ur}
2A46V	89	27	62	72.1	709	81.1	797
3A46V	108	30	78	60.2	592	65.7	645
4A46V	117	34	84	48.5	476	50.3	495
3B46W	108	37	71	60.1	581	67.4	652
3B38W	121	37	84	44.6	593	50.6	673
2C46V	108	40	68	86.4	850	92.2	907
3C46V	139	46	93	72.3	710	70.6	694
4C46V	137	47	90	54.4	535	55.3	544
5C46V	127	51	76	40.3	396	38.8	382
6C46V	108	50	58	29.5	290	32.0	314
3D46V	138	55	83	73.8	725	77.7	764
4D46V	141	60	81	55.4	545	56.4	555
5D46V	115	61	54	39.8	392	40.7	400
6D46V	83	61	22	26.5	261	28.5	280
7D46V	123	66	57	30.8	303	32.0	315
5C36V	132	50	82	22.6	340	22.3	336
5C62V	108	46	62	60.1	379	58.8	371
2C35V	139	42	97	52.8	843	53.9	859
3C35X	160	44	116	39.9	636	40.7	648
5C76V	106	44	62	84.7	407	81.1	389
5C46Y	119	49	70	38.3	377	39.3	386
5C76Z	92	42	50	73.1	352	73.7	354
5C46V*	147	50	97	45.1	443	45.2	444
4C46V*	136	47	89	51.9	510	53.1	522
5C62V*	135	45	90	77.3	488	77.8	491
3C35X*	158	41	117	38.9	621	43.1	686
2B35V*	130	29	101	46.2	742	48.5	773

Table 8 Rupture beam data

Beam number and order of casting and testing	Side in Flexural Tension	Machine Load kips	Shear kips	Moment in·kips	Flexural Stress psi
RB 1	Top	24.5	12.25	269.5	337
RB 2	Bottom	31.0	15.5	341.0	427
RB 3	Top	29.8	14.9	327.8	410
RB 4	Bottom	33.3	16.65	366.3	458
RB 5	Top	29.4	14.7	323.4	405
RB 6	Bottom	32.4	16.2	356.4	446

$$f'_c = 3760 \text{ psi}$$

$$f'_t = 469 \text{ psi} = 7.65\sqrt{f'_c}$$

Average top cast flexural stress = 384 psi = $6.26\sqrt{f'_c}$

Average bottom cast flexural stress = 444 psi = $7.25\sqrt{f'_c}$

$$\frac{\text{Bottom } \bar{\sigma}_{ave}}{\text{Top } \bar{\sigma}_{ave}} = 1.16$$

Table 9 Parameters used in multiple regression analysis

Specimen	$\frac{V}{bd}$	$\frac{M}{Vpd}$	$\sqrt{f'_c}$	G	L''	$\frac{bd\sqrt{f'_c}}{V}$	$\frac{M\sqrt{f'_c}}{Vpd}$	$\frac{MG}{VpdL''}$	$\frac{bdA_s}{V}$
2A46V	430	172.81	56.3	1.25	46	0.1313	9729.58	4.696	0.00466
3A46V	521	115.21	58.1	1.55	46	0.1117	6687.88	3.882	0.00577
4A46V	563	85.96	61.0	1.98	46	0.1082	5242.64	8.700	0.00710
3B46W	402	151.14	56.4	1.25	46	0.1404	8522.94	4.1069	0.00747
3B38W	450	109.73	55.6	1.25	38	0.1235	6099.69	3.6095	0.00666
2C46V	347	259.21	59.3	1.25	46	0.7710	15357.11	7.004	0.00577
3C46V	446	172.81	64.8	1.25	46	0.1452	11199.26	4.696	0.00672
4C46V	439	129.61	62.1	1.34	46	0.1412	8052.29	3.775	0.00909
5C46V	407	103.68	65.6	1.58	46	0.1608	6799.08	3.5613	0.01226
3D46V	333	230.41	60.1	1.25	46	0.1808	13843.85	6.2610	0.00903
4D46V	340	172.81	62.9	1.25	46	0.1852	10860.83	4.6957	0.01178
5D46V	277	138.25	62.1	1.30	46	0.2242	8577.98	3.9068	0.01805
6D46V	201	115.21	58.4	1.40	46	0.2921	6727.45	3.5062	0.03001
7D46V	297	98.16	60.9	1.63	46	0.2056	5979.10	3.4783	0.02363
5C36Y	424	67.56	64.1	1.58	36	0.1512	4331.08	2.9650	0.01180
5C62Y	347	161.49	64.7	1.58	62	0.1866	10453.18	4.1152	0.01442
2C35V	447	159.86	62.1	1.25	35	0.1391	9932.09	5.7093	0.00448
3C35X	514	106.58	62.1	1.25	35	0.1208	6612.81	3.8062	0.00584
5C76V	341	212.07	66.1	1.58	76	0.1942	14002.81	4.4086	0.01469
5C46Y	382	103.68	61.6	1.58	46	0.1612	6391.57	3.5713	0.01308
5C76Z	286	212.07	62.8	1.58	76	0.2126	13311.29	4.4086	0.01692
5C46V*	472	103.68	63.2	1.58	46	0.1339	6552.57	3.5614	0.01059
4C46V*	437	129.61	62.0	1.34	46	0.1419	8035.82	3.7755	0.00915
5C62V*	433	161.49	62.9	1.58	62	0.1453	10157.72	4.1148	0.01155
3C35X*	508	106.58	57.2	1.25	35	0.1126	6096.38	3.8060	0.00591
2B35V*	626	106.58	60.8	1.25	35	0.0971	6480.06	3.8060	0.00319

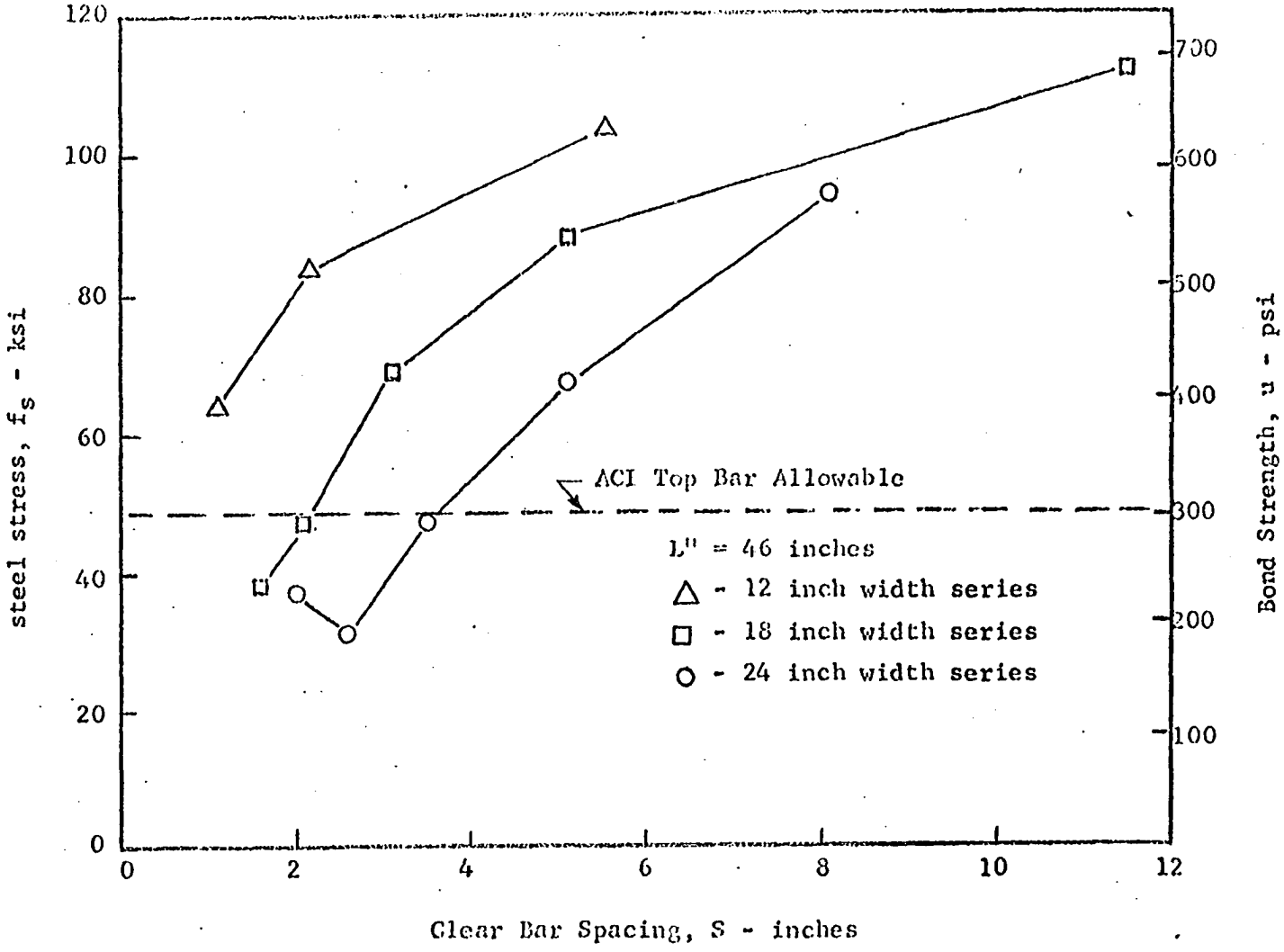

Fig. 18. Steel stress and bond strength versus clear bar spacing

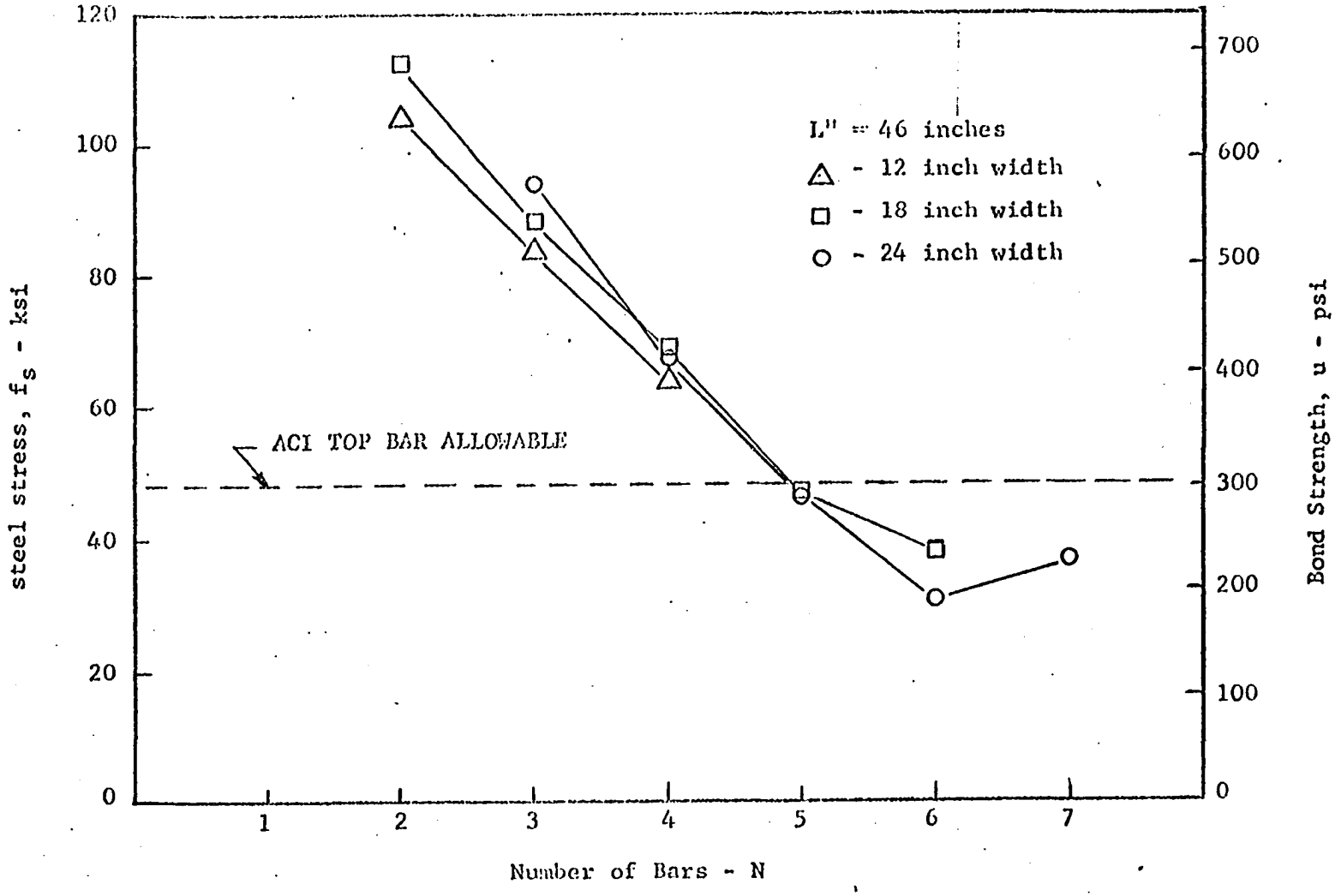

Fig. 19. Steel stress and bond strength versus number of bars

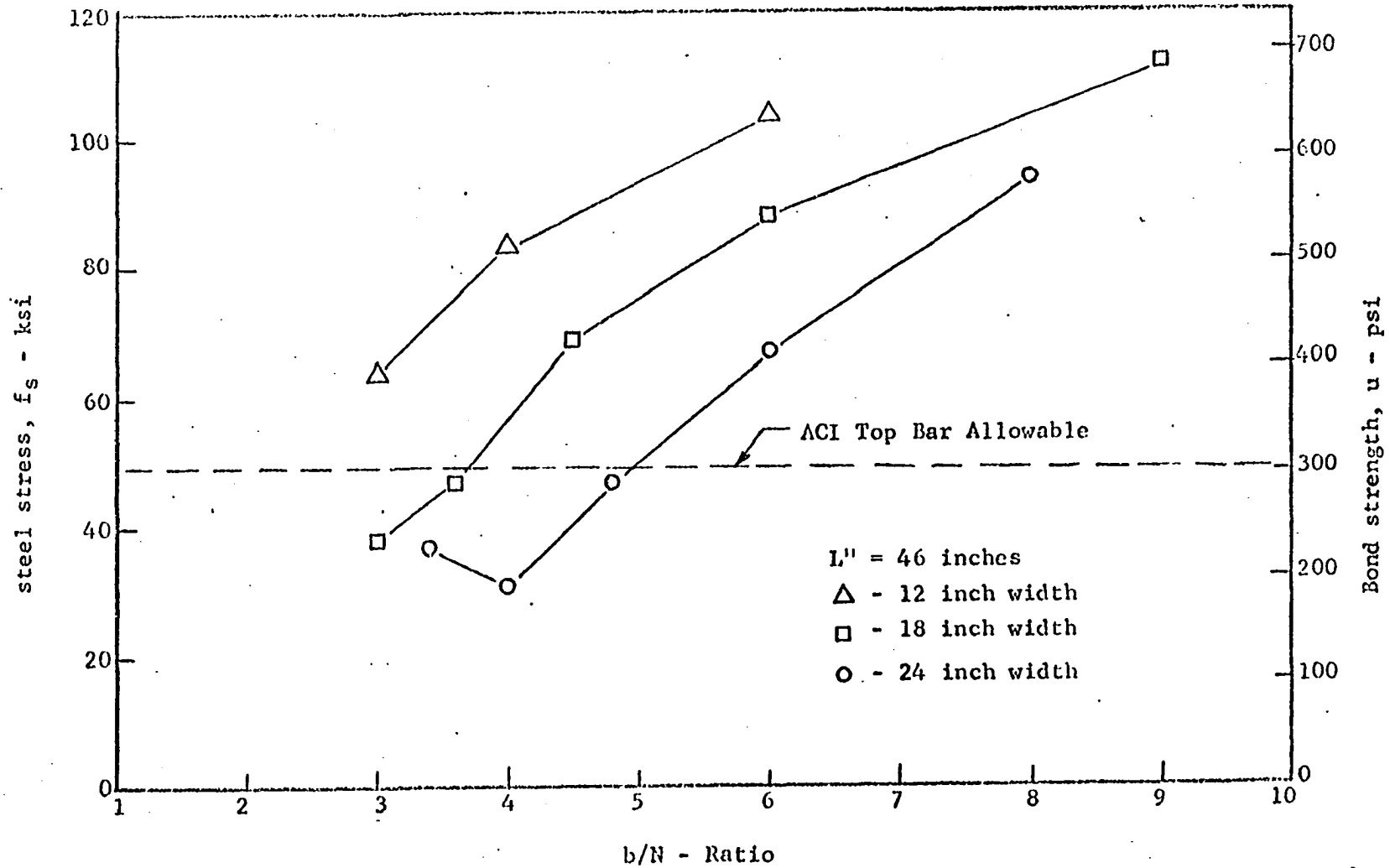

Fig. 20. Steel stress and bond strength versus the ratio, b/N

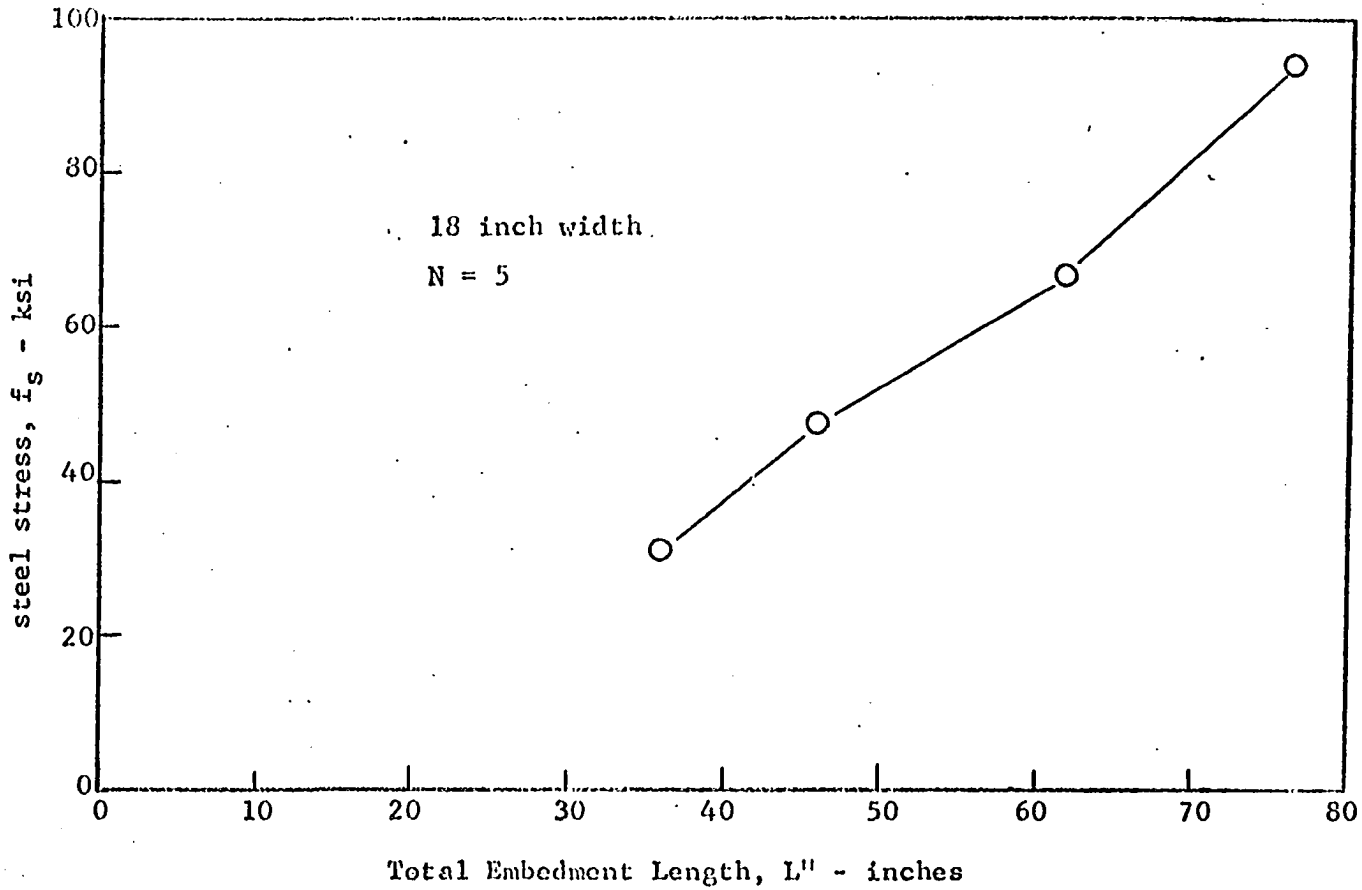

Fig. 21. Developed steel stress versus total embedment length

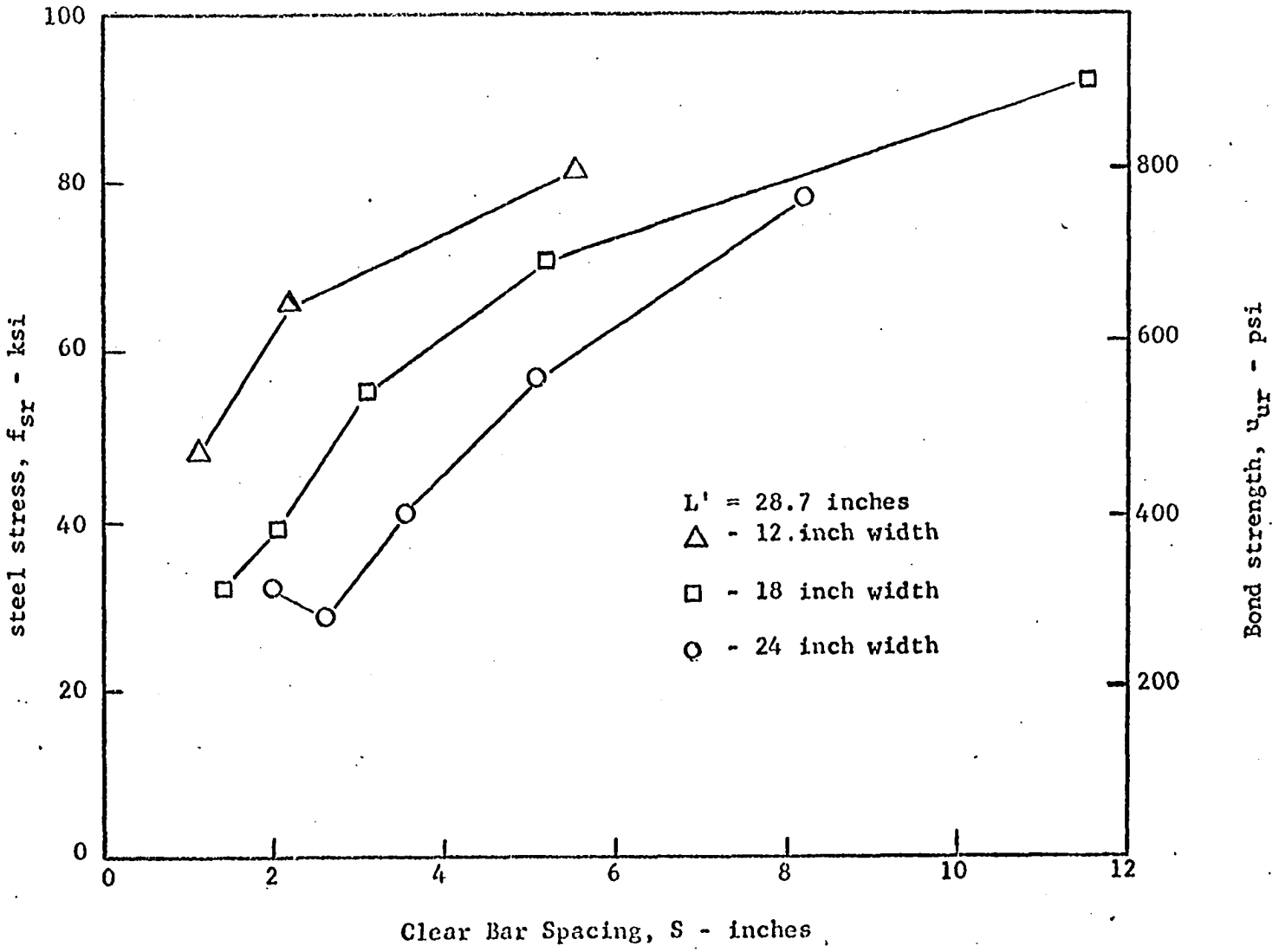

Fig. 22. Developed steel stress versus clear bar spacing considering redistribution

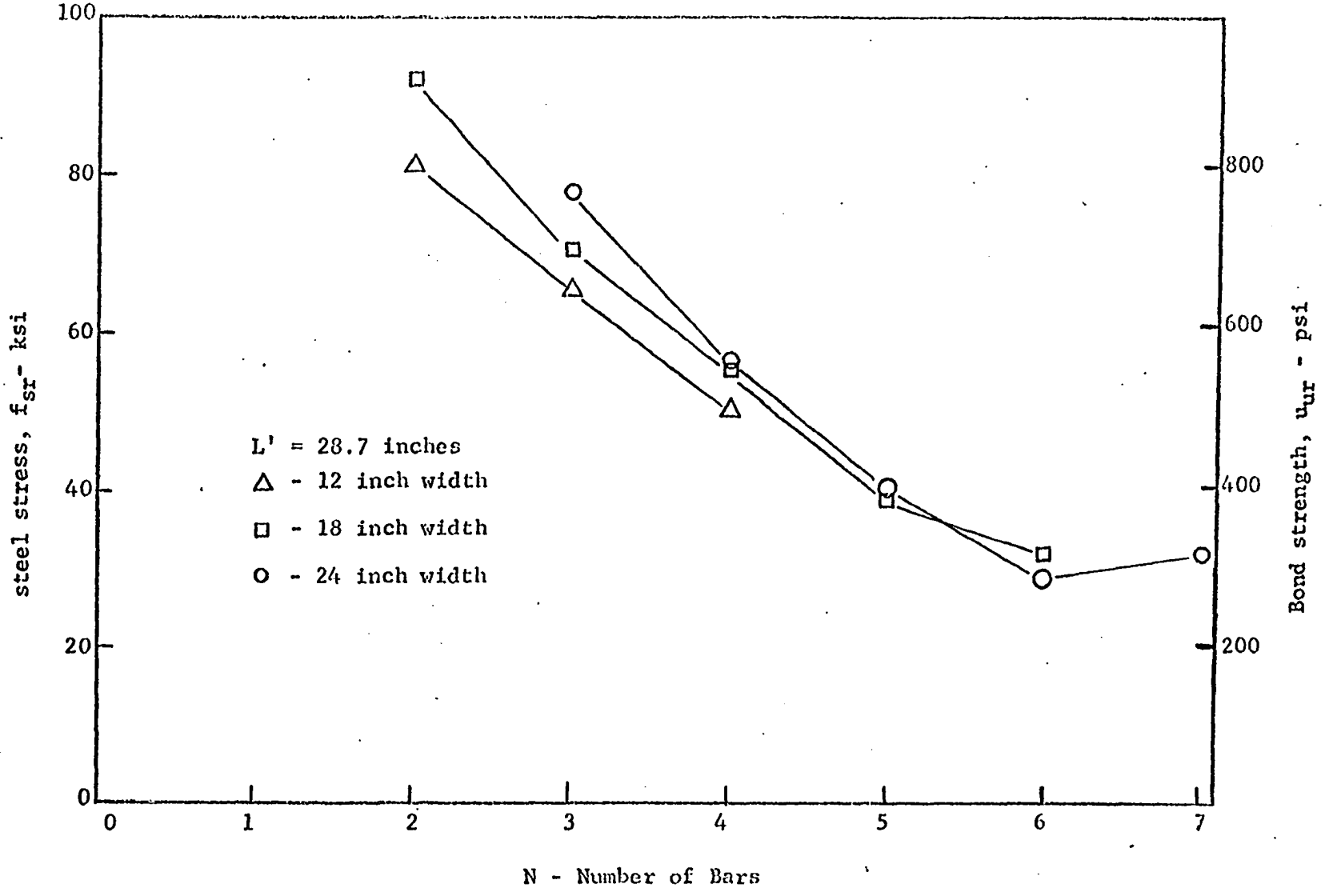

Fig. 23. Developed steel stress versus number of bars per beam considering redistribution

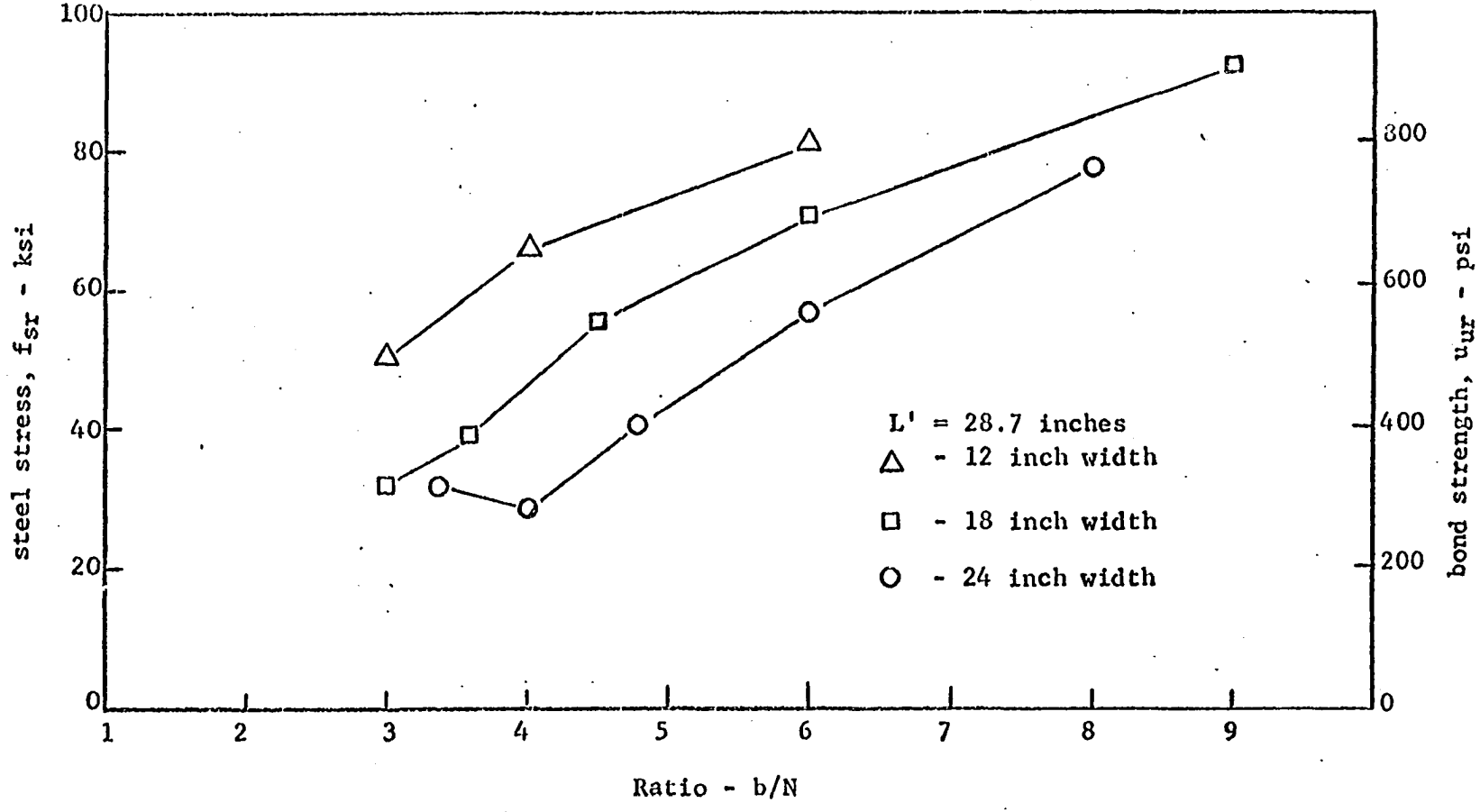

Fig. 24. Steel stress and bond strength versus b/N considering redistribution

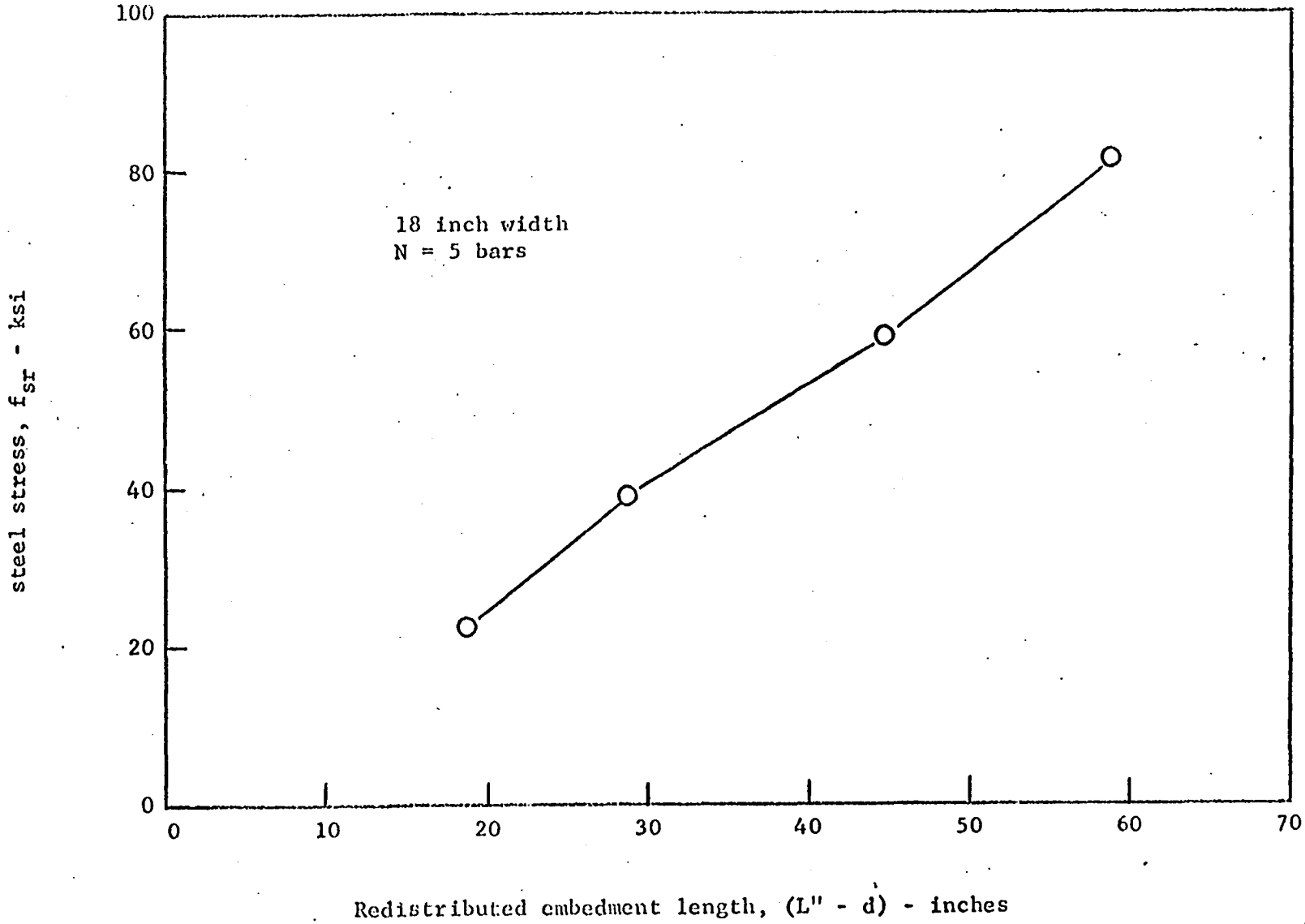

Fig. 25. Steel stress versus embedment length considering redistribution

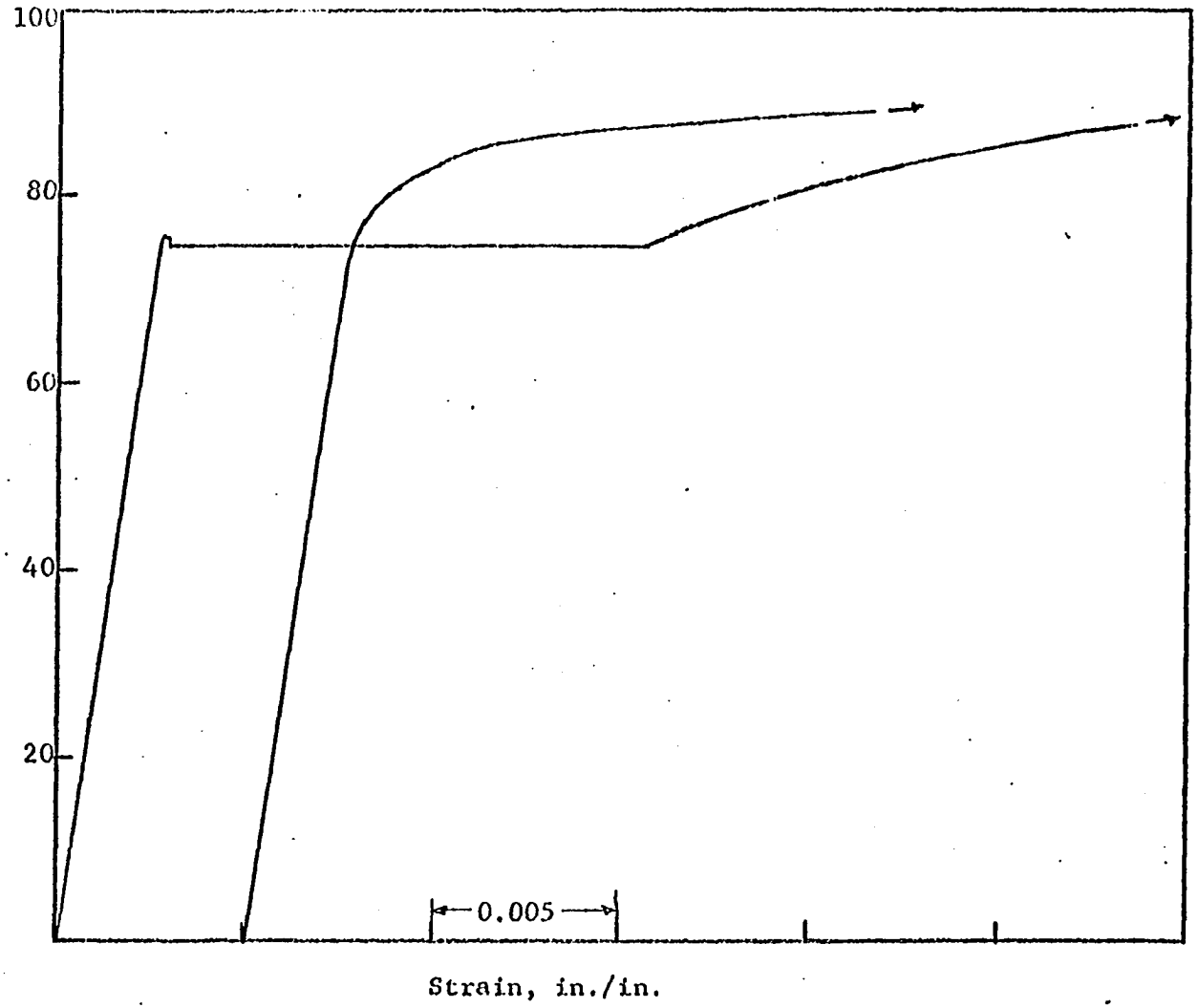

Fig. 26. Typical stress-strain curves for longitudinal reinforcement

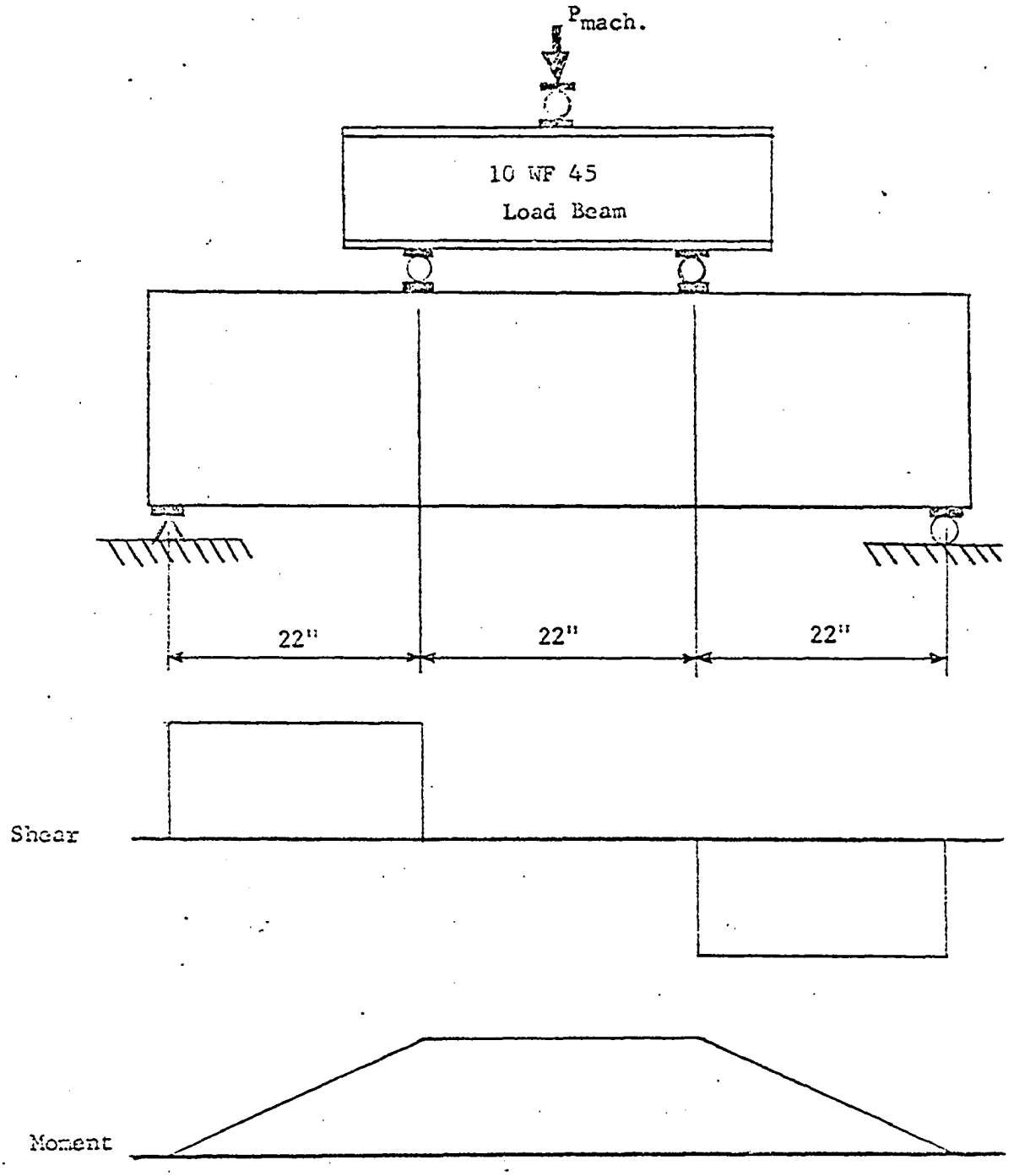

Fig. 27. Modulus of rupture beam and load arrangement

APPENDIX B: PHOTOELASTICITY INVESTIGATION OF RADIAL STRESSES

Introduction

The purpose of this portion of the program was to study the effect of the normal radial stresses acting in planes perpendicular to the longitudinal axis of the reinforcing bars (Fig. 1). The effect of radial stresses was used in a semi-rational analysis of anchorage failures. In particular, the maximum tangential elastic stress concentration ratio was to be determined on the boundary of the holes made by reinforcing bars as a function of bar spacing using a plane stress case. The stress concentration ratio was defined as the ratio of the boundary tangential stress to the applied normal radial pressure. The photoelastic technique furnished a relatively quick and easy means of determining such information. Models were prepared to represent cross sections of the concrete beams tested.

The theory of the photoelastic method, its equipment and procedures have been treated in numerous articles and texts (5, 6). The 15 inch diameter diffused light polariscope, equipped with a monochromatic sodium light source and other equipment used were basically the same as described in Dally and Riley's EXPERIMENTAL STRESS ANALYSIS.

In two-dimensional photoelasticity, a photoelastic model under load in the field of a circular polariscope produces isochromatic fringe patterns. These fringes are dark bands along which the principal stress difference, $(\sigma_1 - \sigma_2)$, is constant. Photographs of dark fields (Figs. 30 and 32) show full order fringes, while photographs of light fields (Figs. 31 and 33) indicate half order fringes. When fringe order, F, at points of interest are established, it is possible to compute the principal stress difference.

$$\sigma_1 - \sigma_2 = \frac{F f_\sigma}{h}$$

where f_σ is the material fringe value and h is the model thickness.

Models and Loading Arrangement

With the aid of superposition the problem of determining the tangential stress at the holes' boundaries was relatively simple (Fig. 28). The internal stresses caused by the hydrostatic stress (Fig. 28a) cause no fringe patterns in the field of the polariscope since $\sigma_1 = \sigma_2$. Therefore, the fringe patterns obtained from the loading in Fig. 28b and the loading of Fig. 28c are identical. In the actual test arrangement, the model was loaded by applying a uniform compressive loading along the boundaries of the model. However, the fringe patterns obtained from the model were identical to those that could be produced by loading in Fig. 28b and 28c since fringes are a measure of the absolute value of principal stress difference.

Loading system

Uniform pressure was applied to the external boundary of the models by means of a loading frame (Fig. 29) and a hydraulic pressure system. Although pressures of 5000 psi could be developed in the pressure system, 1000 psi was used as a maximum test pressure because buckling began to occur at 1500 psi. Hydraulic fluid was contained within the loading frame by a 5/16 inch rubber latex hose which was anchored near the point of entry after traversing the model. The other end of the rubber hose extended into a copper pipe for about 4 inches and it was held there by friction while under pressure. The copper pipe which was anchored in the top plate of the loading frame was then connected to a hydraulic pressure line. Under pressure the rubber

tube was confined on three sides by the loading frame and on the fourth side by the photoelastic model which was to have the uniform pressure applied.

Models

Models were prepared from Columbia Resin CR 39 material which was 1/4 inch thick. Models were constructed by first rough cutting with a band saw and then finishing the edge surfaces to the same form as the model template with a high speed router.

Beam cross sections with 12 and 18 inch widths were modeled. Holes were routed to represent 2, 3, 4 and 7 bars for the 18 inch width series at 1/3 scale. Holes to represent 2, 3, and 4 bars for the 12 inch wide series at 1/2 scale were made.

For each model a standard circular calibrating disc was prepared at the same time from an area of the same sheet of CR 39 adjacent to that in which the model was prepared. The circular discs were 2 1/2 inches in diameter. These discs were used to determine the material fringe values, f_σ. Material fringe values varied from 95 to 100 psi•inch per fringe.

Results

Photographs of typical fringe patterns are shown in Figs. 30 through 33. Boundary stresses were determined from fringe orders, F, and

$$\sigma_1 - \sigma_2 = \frac{Ff_\sigma}{h}$$

Since, in this case on the boundary of the hole, σ_2 equals the applied pressure, -f, the tangential stress on the boundary of the hole is

$$\sigma_1 = \frac{Ff_\sigma}{h} - f$$

The tangential stress concentration ratio, G, is the ratio of σ_1 to f.

$$G = \frac{Ff_\sigma}{hf} - 1$$

Figure 34 contains plotted curves showing maximum tangential stress concentration, G, on interior and exterior holes plotted against clear spacing between holes, S, expressed in hole diameters. Note that interior holes produce the maximum stress concentration ratio at spacings greater than 2.4D. This is due to the fixed clear cover of approximately 2.3D. Clear spacing in excess of three hole diameters produces no significant change in maximum stress concentration on the holes' boundaries.

Plotted in Figs. 35 and 36 are typical tangential stress concentration ratio distributions about the boundary of corner and interior holes respectively. For the plots of Fig. 35, the holes were spaced at 10.19D, 1.93D, and 0.86D. In Fig. 36, hole spacing was 2.75D, 1.93D, and 0.86D. The angle, α, is defined as shown in each figure.

For corner or exterior holes, maximum tangential stress concentration occurred in the 1st and 3rd quadrant, i.e. $\alpha \cong 75^\circ$ and 250°, for widely spaced holes, while for closer spaced bars maximum stress concentration occurred at $\alpha = 0^\circ$ or on the hole's boundary adjacent to the interior holes.

For the interior holes, close spacing produced high stress concentration at the holes' boundaries along a horizontal plane, i.e. $\alpha = 0^\circ$ and 180°. As the spacing increased the fringe patterns became more circular and the stress concentration more uniform about the circumference of the interior holes.

It would appear from the above results, that initial splitting due to radial stresses would occur on a horizontal plane between interior reinforcing bars when the bars are closely spaced. With the cover and bar diameter

used in this program, closely spaced would be a clear spacing of less than 2.4D. For bar spacing greater than 2.4D initial splitting would be through the cover adjacent to the outside bar.

a) Hydrostatic state of stress

b) Uniform tensile loading applied to external boundaries

c) Internal radial loading applied to hole boundaries

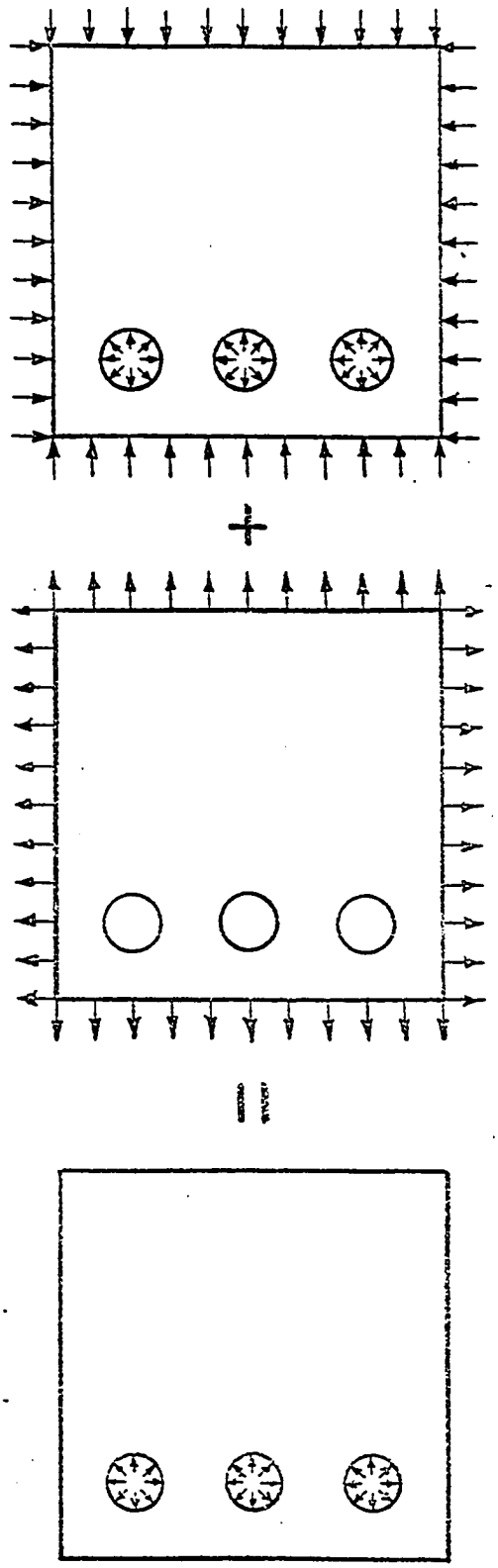

Fig. 28. Superposition of loading to obtain radial stresses on boundary of holes

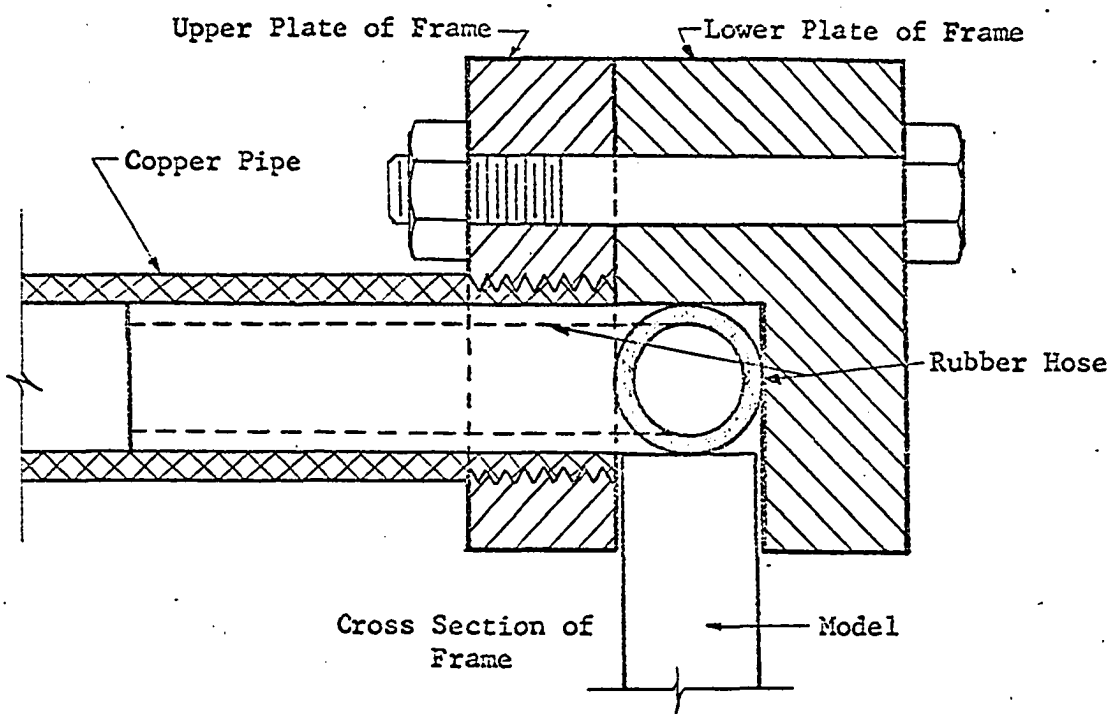

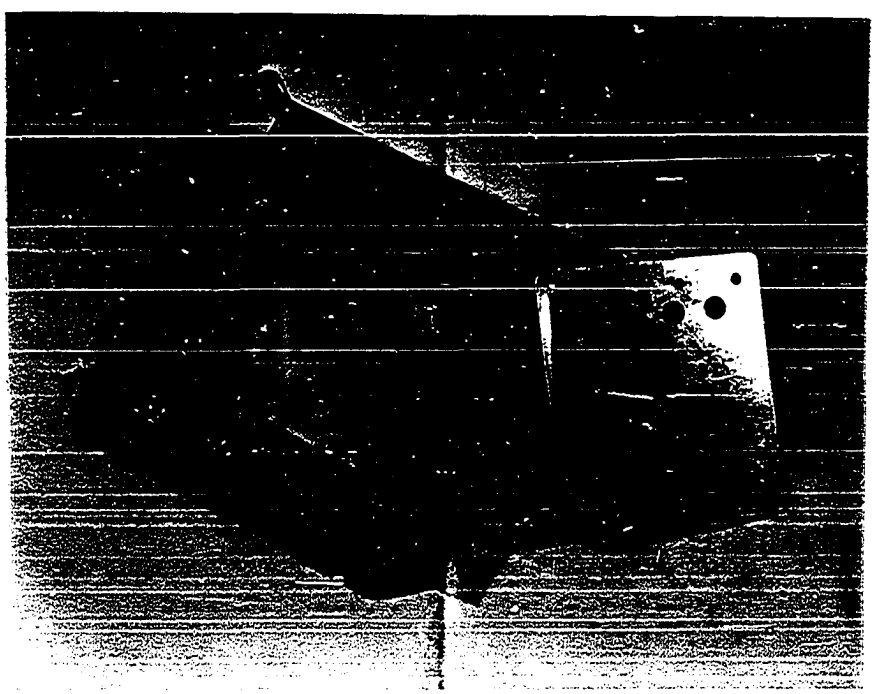

Fig. 29. Loading frame, model, and model template

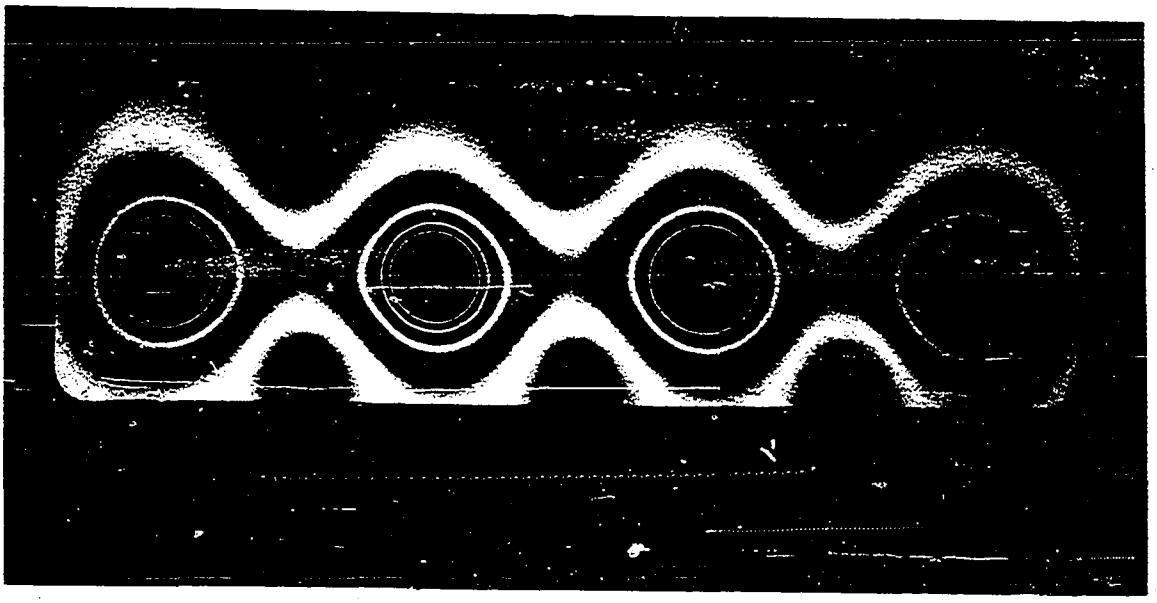

Fig. 30. Dark field fringe pattern (S = 2.75D)

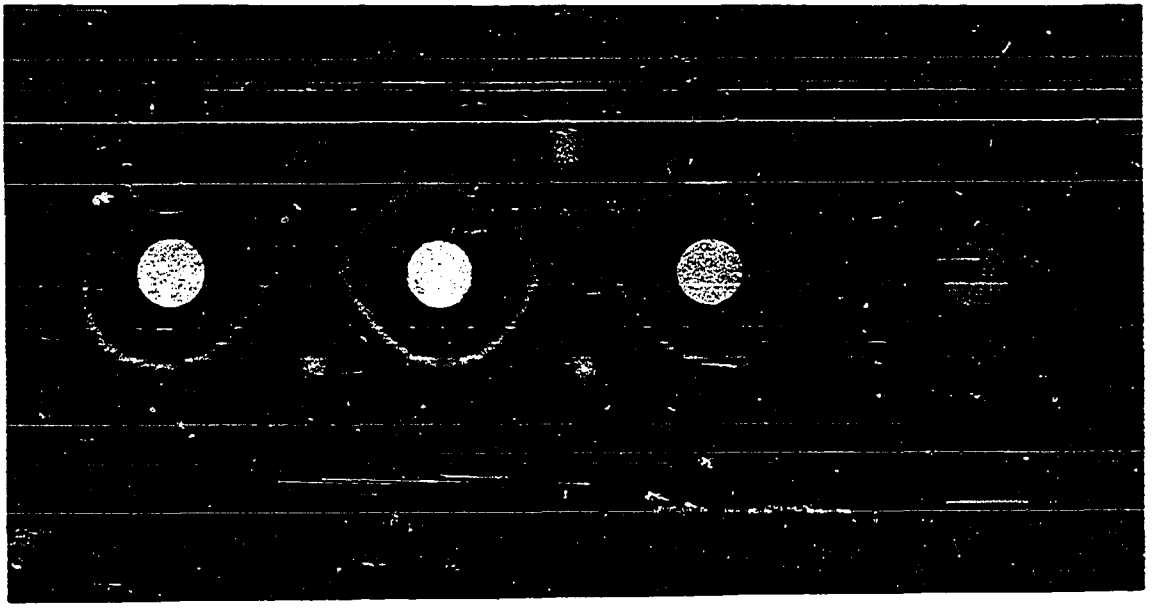

Fig. 31. Light field fringe pattern (S = 2.75D)

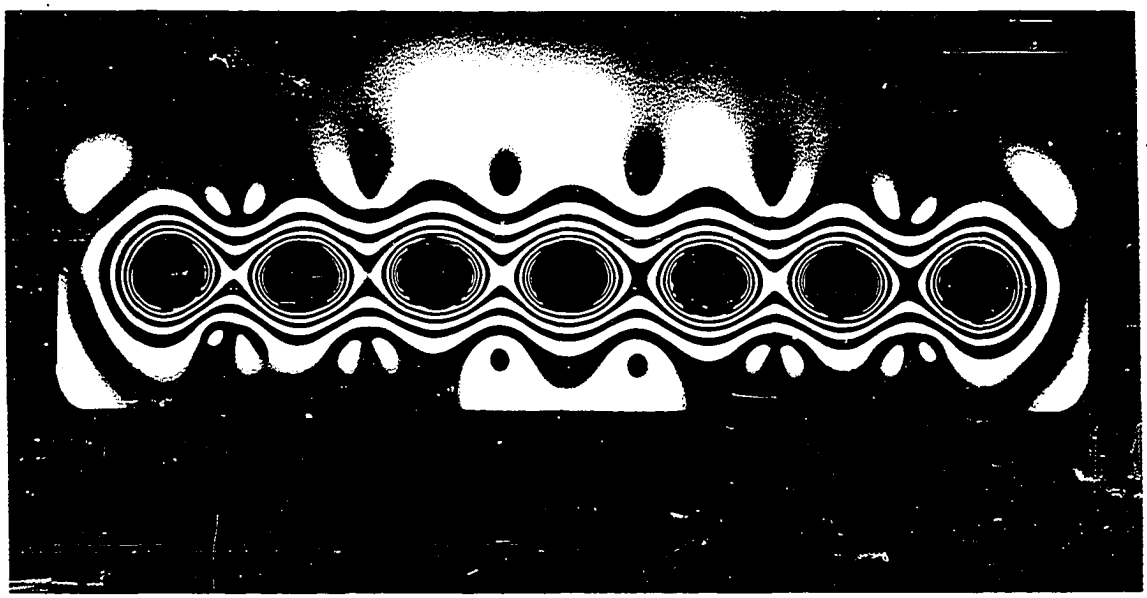

Fig. 32. Dark field fringe pattern (S = 0.86D)

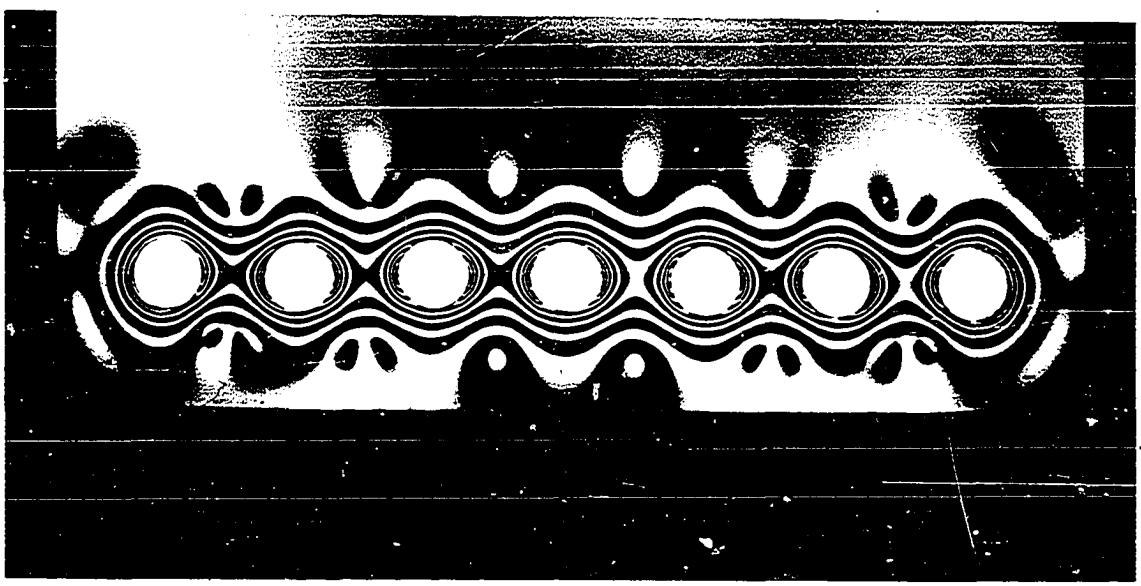

Fig. 33. Light field fringe pattern (S = 0.86D)

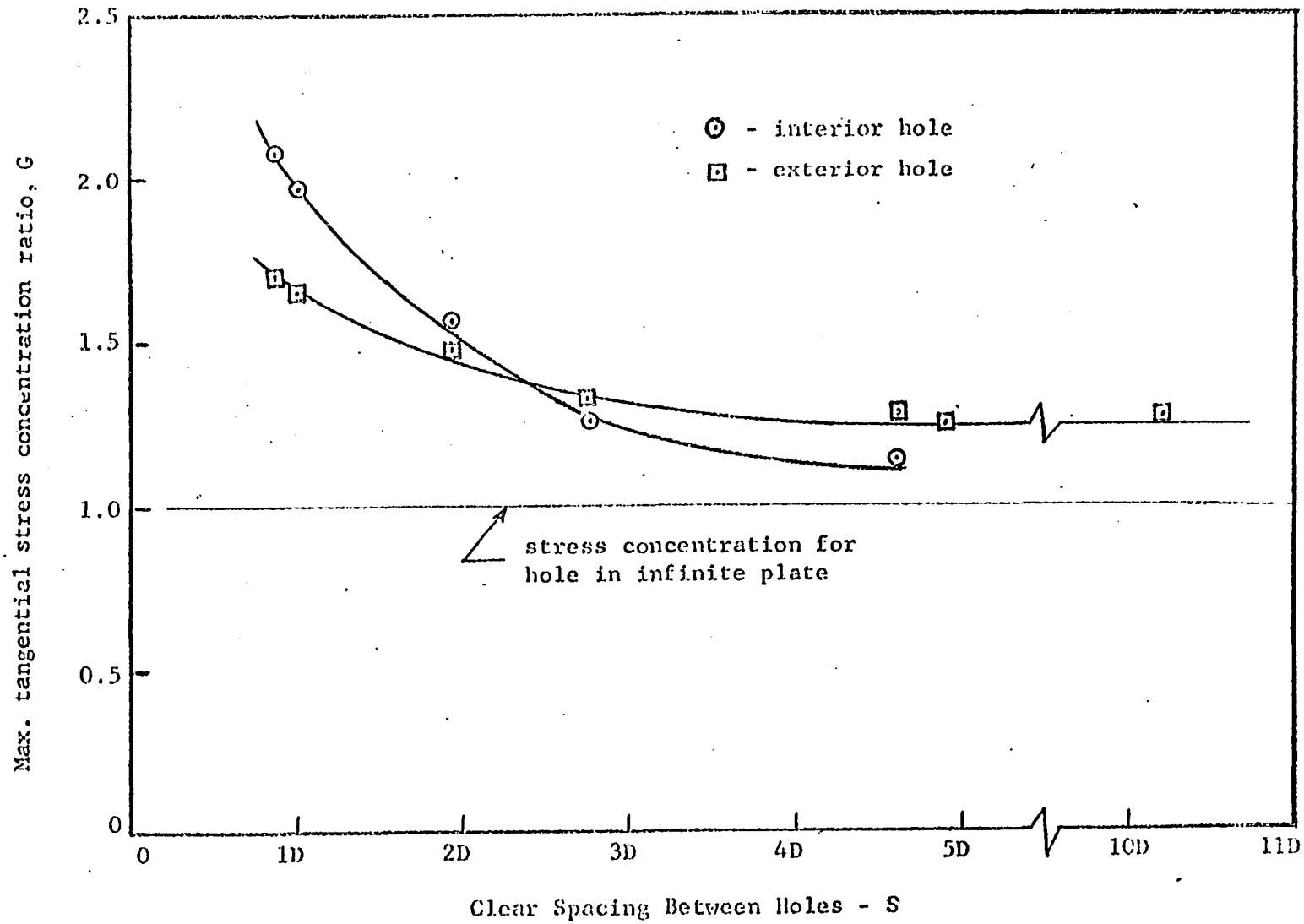

Fig. 34. Maximum tangential stress concentration ratio versus clear spacing of holes

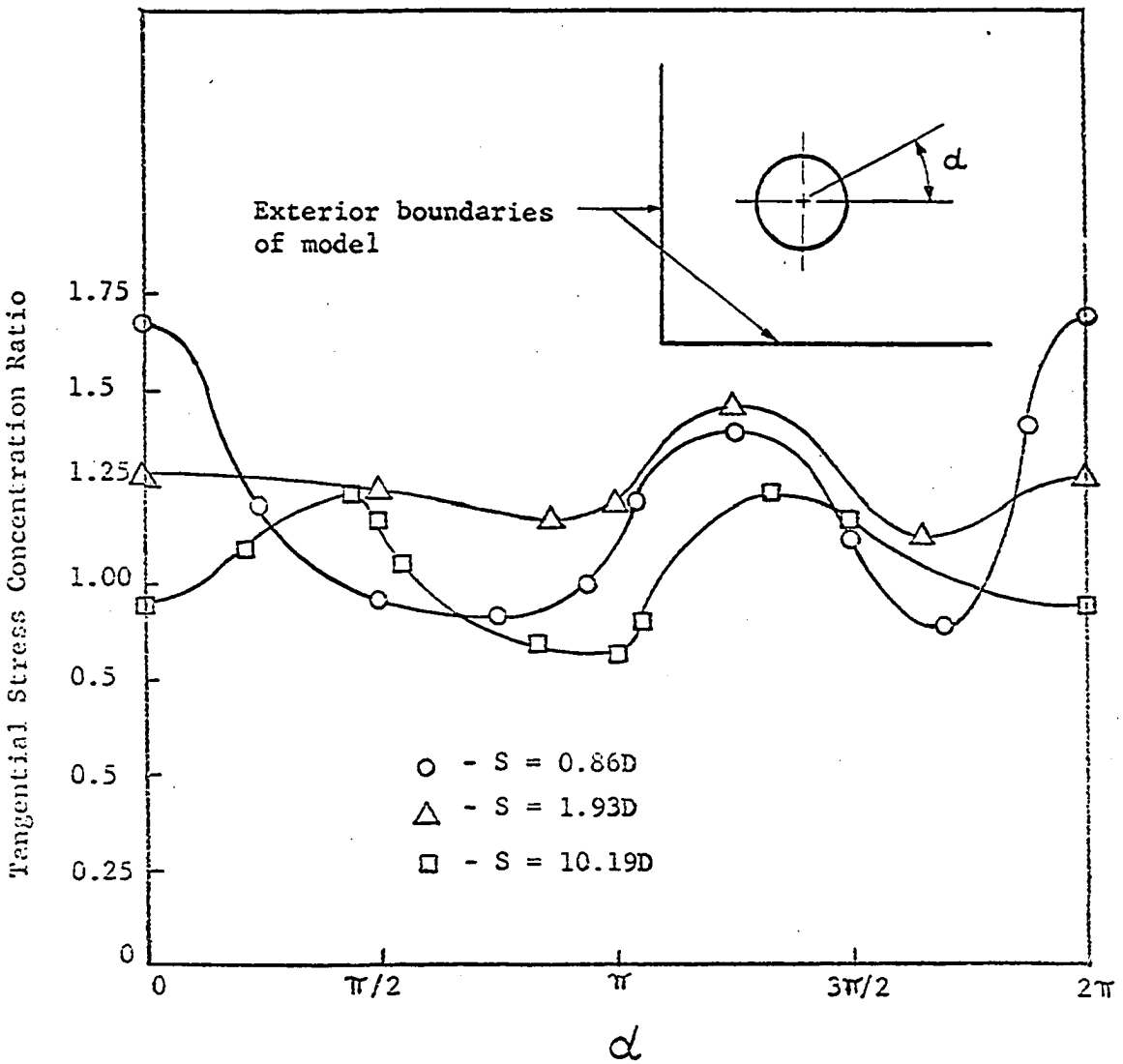

Fig. 35. Tangential stress concentrations about circumference of corner hole

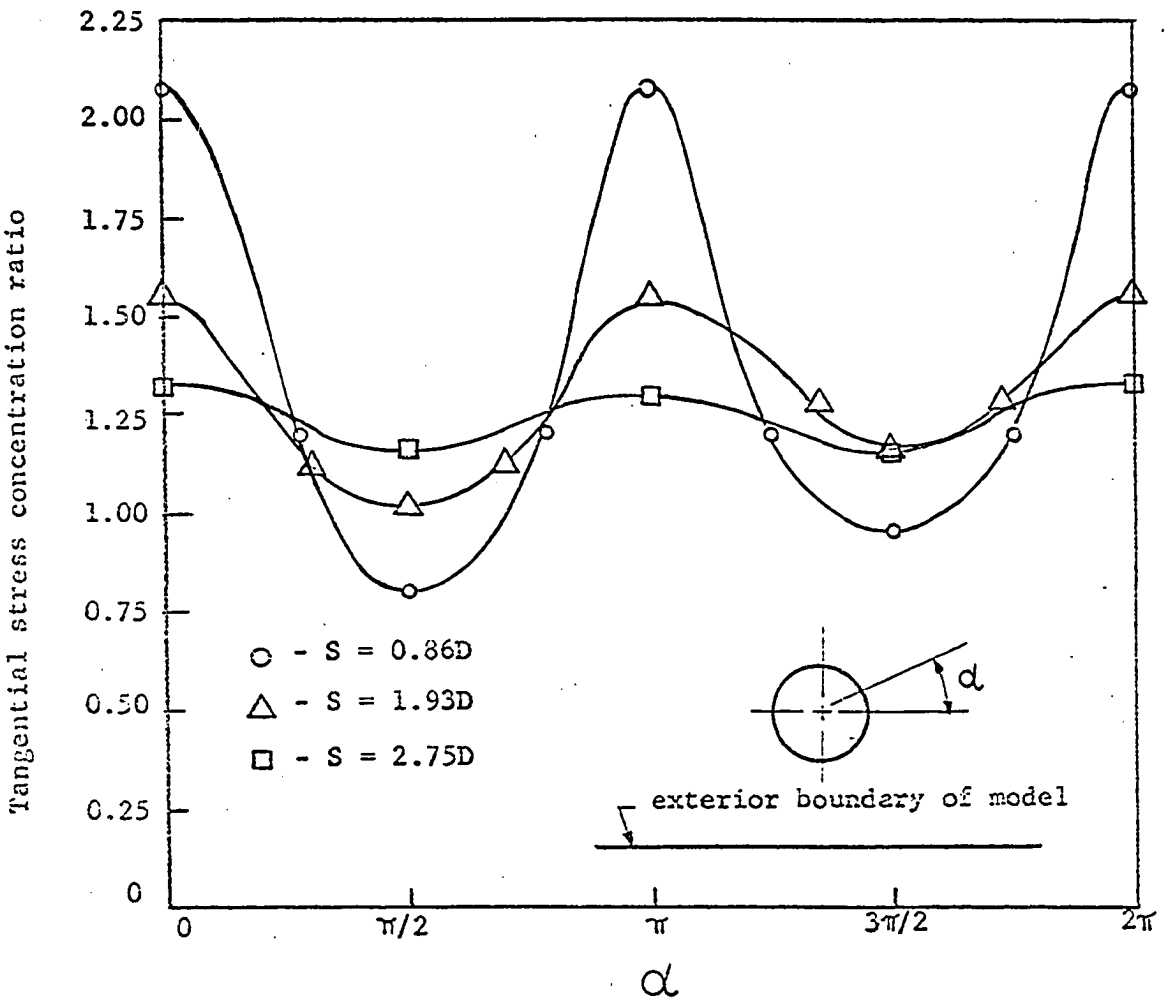

Fig. 36. Stress concentration ratios about the circumference of center interior holes